# On the ASEP of Decode-and-Forward Dual-Hop Networks with Pilot-Symbol Assisted $M$-PSK

Nikos C. Sagias, *Senior Member, IEEE*

***Abstract*—We develop an analytical framework for the end-to-end (e2e) average symbol error probability (ASEP) of dual-hop relaying networks with pilot-symbol assisted $M$-ary phase-shift keying ($M$-PSK) modulation. The relays use the selective decode-and-forward protocol and are equipped with multiple receive antennas. The channels are estimated per antenna branch based on the least-squares estimation (LSE) technique by means of pilot symbols. Also, maximal-ratio combining and coherent detection are performed per receiving end. Exact e2e analytical ASEP expressions are derived for binary and quadrature phase-shift keying (BPSK and QPSK), while simple approximate expressions and bounds are obtained for high signal-to-noise ratio (SNR) when $M \geq 2$. Our analysis is generic enough to account for any frequency-flat, time-selective, and/or arbitrarily correlated fading channel model per hop. As a case study, we further provide e2e ASEP expressions considering arbitrarily correlated Nakagami fading channels. For high SNR, closed-form expressions are derived, while the cooperation-gain and diversity-order are also extracted. In addition, two power allocation strategies are investigated and analytical solutions are provided. Comparisons between numerical and computer simulation results are finally presented to verify the validity of the proposed approach and the accuracy of the high-SNR approximate expressions.**

***Index Terms*—Average symbol error probability (ASEP), channel state information (CSI), cooperative communications, correlated fading, decode-and-forward (DF), imperfect channel estimation (ICE), least-squares estimation (LSE), $M$-ary phase-shift keying ($M$-PSK), maximal-ratio combining (MRC), optimal power allocation (OPA), pilot-symbols assisted modulation (PSAM), relays.**

## I. Introduction

COOPERATIVE communication networks promise high quality of services for contemporary and next-generation communication systems [1]. Their end-to-end (e2e) performance can be further improved by employing multiple antennas relays and using efficient combining schemes. A reasonable choice is the maximal-ratio combining (MRC) scheme, that maximizes the instantaneous output signal-to-noise ratio (SNR), and consequently, offers the best error rate performance. For coherent detection based on this scheme channel estimates are required. In practice, these estimates are imperfect. Specifically, noise is added to them, due to the channel estimation technique used, resulting in performance degradation. It is, therefore, important to study the effect of such imperfections on the e2e performance and optimize critical parameters, such as the pilot symbols power, number of pilots per channel block, number of relays and antennas, etc., to compensate for the degradation.

In the open technical literature there are many important works on point-to-point communications considering pilot-symbols assisted modulation (PSAM) techniques, e.g., [2]–[8]. Motivated by these early works, various papers on cooperative communications with imperfect channel state information (CSI) have been published [9]–[18]. For example in [14] the impact of imperfect transmitter CSI on the diversity gain has been investigated assuming dynamic decode-and-forward (DF) relaying channels, while an analysis for the diversity and multiplexing tradeoff has been also presented. The effect of outdated channel estimates on DF relay selection, when operating over Nakagami-$m$ fading channels has been studied in [15], where closed-form expressions for the e2e outage probability have been derived. The performance of a multi-hop wireless communication system with arbitrary number of intermediate relays has been analyzed in [19] assuming Rayleigh fading and the DF relaying protocol. Recently in [18], the quadrature phase-shift keying (QPSK) average bit error probability (ABEP) of a cooperative network with adaptive DF relaying and PSAM over time-selective and frequency-flat Rayleigh fading has been studied. Although the aforementioned works cover important aspects of DF cooperative systems with imperfect CSI, specific assumptions are being made that limit their generality, e.g., by assuming a specific channel model, a single-channel scenario, uncorrelated channels, or a specific modulation order.

In the current work a different approach is followed to analyze the performance of dual-hop networks under imperfect CSI. As it is reported in [20, Appendix C], the error rate performance of $M$-ary phase-shift keying ($M$-PSK) systems, can be analyzed directly from the distribution of the inner product of two complex Gaussian random vectors. Following this approach, a key point in our analysis is the generalization of a theorem originally presented in [8], [21] for the joint characteristic function (CF) of the real and imaginary parts of the inner product of two independent complex Gaussian random vectors. This preliminary step is required in order to consider not-necessarily identical transmission powers for each relay. Based on this generalization, we develop a unified analytical framework for the e2e $M$-PSK error-rate performance of dual-hop and multi-relay cooperative networks. The selective-DF protocol is adopted, while we consider that the relays are equipped with an arbitrary number of receive antennas. Prior to data transmission, each relay estimates the CSI using the least-squares estimation (LSE) technique by means of pilot symbols. Then, coherent detection based on the MRC scheme is performed. The inner-product

Manuscript received July 23, 2013; revised November 2, 2013. The editor coordinating the review of this paper and approving it for publication was C. Abou-Rjeily.

This work was funded by the University of Peloponnese in the context of internal project ODesRI. Part of this paper was presented at the IEEE Wireless Communications & Networking Conference, Istanbul, Turkey, Apr. 6-9, 2014.

N. C. Sagias is with the Department of Informatics and Telecommunications, University of Peloponnese, end of Karaiskaki street, 22100 Tripoli, Greece (e-mail: nsagias@ieee.org).

Digital Object Identifier 10.1109/TCOMM.2014.011814.130556

approach appears to be a powerful tool, since it has the advantage of generality. Specifically, our analytical framework can be exploited assuming any time- and space-correlated channel model per hop, not-necessarily identical channels, and arbitrary number of antennas per receiving end. The only requirement is that the CF of the sum of squared fading envelopes for the channel model under consideration should be available. Fortunately, for the most popular channel models, e.g., Rayleigh, Rice, and Nakagami, such an expression is readily available [8, eqs. (51) and (63)]. In order to demonstrate the generality of our analytical framework, we further consider arbitrarily correlated Nakagami fading for each hop. Exact closed-form as well as analytical average symbol error probability (ASEP) expressions are presented for binary phase-shift keying (BPSK) and QPSK, respectively, while accurate high-SNR approximate expressions are obtained for any order $M$-PSK modulation formats. These expressions help us to extract the cooperation-gain and diversity-order. Two different power allocation strategies are also investigated and analytical solutions are provided.

The rest of this paper is organized as follows. The next section presents the system and channel models for the cooperative network under consideration. In Section III general analytical expressions for the e2e $M$-PSK ASEP are extracted, while specific formulas are obtained assuming correlated Nakagami fading channels. Section IV presents further results concerning the cooperation-gain and diversity order, while a per node and a joint power allocation strategy are also investigated. In Section V numerical and computer simulation results are provided, while concluding remarks are given in Section VI.

Notations: $\mathbf{I}_L$ is the $L \times L$ identity matrix, $\mathbf{1}_L$ and $\mathbf{0}_L$ denote $L \times 1$ vectors of ones and zeros, respectively, $\otimes$ denotes the Kronecker product of matrices, $(\cdot)^T$ and $(\cdot)^H$ denote the transpose and Hermitian operators, respectively, $\mathbf{x} \sim \mathcal{CN}(\boldsymbol{\mu}_\mathbf{x}, \mathbf{K}_\mathbf{x})$ reads as "$\mathbf{x}$ is distributed as a complex normal vector with mean and covariance matrix $\boldsymbol{\mu}_\mathbf{x} = \mathcal{E}_\mathbf{x}\langle\mathbf{x}\rangle$ and $\mathbf{K}_\mathbf{x} = \mathcal{E}_\mathbf{x}\langle(\mathbf{x}-\boldsymbol{\mu}_\mathbf{x})(\mathbf{x}-\boldsymbol{\mu}_\mathbf{x})^H\rangle$, respectively," with $\mathcal{E}_\mathbf{x}\langle\cdot\rangle$ standing for the expectation over $\mathbf{x}$ operator, $(\cdot)^*$ denotes the complex conjugate, $\mathrm{Tr}\{\cdot\}$ and $\mathrm{Det}(\cdot)$ stand for the trace and the determinant of a matrix, respectively, $\mathrm{Diag}\{\cdot\}$ stands for a square diagonal matrix, $\mathrm{Res}\{\cdot\}$ for the residue of a complex function, $\Re\{\cdot\}$ and $\Im\{\cdot\}$ denote the real and imaginary operators, respectively, $\jmath = \sqrt{-1}$, $\|\cdot\|$ denotes the Euclidean norm, and $\mathbb{R}$ and $\mathbb{C}$ are the set of real and complex numbers, respectively.

## II. Cooperative System and Channel Models

This section presents the cooperative system and channel models under consideration. It also provides the mathematical background for the least-squares channel estimation technique. For the reader's convenience, Table I summarizes the most important mathematical symbols that are included in the analysis follows along with a short description for each one of them.

### A. Dual-Hop Network

We consider a dual-hop network where a source node $\mathcal{S}$ transmits $M$-PSK symbols to a destination node $\mathcal{D}$ both directly and through $R$ relay nodes $\mathcal{R}_1$, $\mathcal{R}_2$, ..., $\mathcal{R}_R$. The source is equipped with one antenna, the destination with $L_0$, and the $p$th relay with $L_p$ ($p = 1, 2, \ldots, R$). The relays use the selective-DF protocol to forward the data received from the source to the destination. According to this protocol a relay forwards the information signal only if it is able to correctly decode it (we shall refer to as *the relay is on*); otherwise it remains idle (we shall refer to as *the relay is off*). The overall $\mathcal{S} \to \mathcal{D}$ transmission of an $M$-PSK symbol is completed in $R+1$ time slots[1]. In the first time slot node $\mathcal{S}$ broadcasts the information signal to $\mathcal{D}$ and to all relays simultaneously. In the next $R$ time slots, each relay forwards the received signal to node $\mathcal{D}$ one-by-one. In our analysis we consider that each relay is able to estimate the receive complex channel gain, while combines the $L_p$ received signals using MRC. The same also holds for the destination node $\mathcal{D}$. Moreover, we shall assume that the destination node is able to verify whether a relay is on or off, for example, using an energy detector.

Let $s \in S$ be the information-bearing symbol that belongs to an $M$-PSK constellation $S = \{S_0, S_1, \ldots, S_{M-1}\}$, with $M$ denoting the modulation order and $S_l = \exp\{\jmath\, 2\pi\, l/M\}$, $l = 0, 1, \ldots, M-1$. Also let $E_\mathrm{s}$ denote the total energy per symbol transmitted by all nodes during $R+1$ time slots. The

TABLE I
A Summary of Mathematical Symbols

| Symbol | Description |
|---|---|
| $\mathcal{S}$ and $\mathcal{D}$ | Source and destination node notation |
| $R$ | Number of relays |
| $\mathcal{R}_p$ ($p = 1, \ldots, R$) | $p$th relay notation |
| $0 < \lambda_\ell < 1$ ($\ell = 0, \ldots, R$) | $\ell$th node transmission power ratio |
| $L_0$ and $L_p$ | Number of antennas of $\mathcal{D}$ and $\mathcal{R}_p$ |
| $\mathbf{V} \in \mathbb{R}^{L_0\,(R+1)\times L_0\,(R+1)}$ | Diagonal matrix, elements: $\sqrt{\lambda_\ell}\,\mathbf{I}_{L_0}$'s |
| $M$ | Modulation order |
| $s$ and $s_{\mathrm{p}_k}$ | Data and $k$th pilot symbol |
| $E_\mathrm{s}$ and $E_\mathrm{p}$ | Total data- and pilot-symbol energy |
| $N_0$ | Noise power spectral density |
| $\gamma$ and $\gamma_\mathrm{p}$ | Average symbol- and pilot-to-noise ratio |
| $\mathbf{w}_p$ | $\mathcal{S} \to \mathcal{R}_p$ receive signal vector |
| $\boldsymbol{\nu}_p \sim \mathcal{CN}\left(\mathbf{0}_{L_p}, N_0\,\mathbf{I}_{L_p}\right)$ | $\mathcal{S} \to \mathcal{R}_p$ link noise vector |
| $\mathbf{g}_p = [g_{p,1}\, g_{p,2} \cdots g_{p,L_p}]^T$ | $\mathcal{S} \to \mathcal{R}_p$ link channel vector |
| $-1 < \varrho_{p,i,j} < 1$ | Correlation coefficient of $g_{p,i}$ and $g_{p,j}$ |
| $\mathbf{r}_\ell$ | $\ell$th node to $\mathcal{D}$ receive signal vector |
| $\mathbf{n}_\ell \sim \mathcal{CN}\left(\mathbf{0}_{L_0}, N_0\,\mathbf{I}_{L_0}\right)$ | $\ell$th node to $\mathcal{D}$ noise vector |
| $\mathbf{h}_\ell = [h_{\ell,1}\, h_{\ell,2} \cdots h_{\ell,L_0}]^T$ | $\ell$th node to $\mathcal{D}$ channel vector |
| $-1 < \rho_{\ell,i,j} < 1$ | Correlation coefficient of $h_{\ell,i}$ and $h_{\ell,j}$ |
| $\mathbf{r} = [\mathbf{r}_0\ \mathbf{r}_1\ \mathbf{r}_2 \cdots \mathbf{r}_R]^T$ | Concatenated receive signal vector |
| $\mathbf{h} = [\mathbf{h}_0\ \mathbf{h}_1\ \mathbf{h}_2 \cdots \mathbf{h}_R]^T$ | Concatenated channel vector |
| $\mathbf{n} = [\mathbf{n}_0\ \mathbf{n}_1\ \mathbf{n}_2 \cdots \mathbf{n}_R]^T$ | Concatenated noise vector |
| $W_\ell$ | $\ell$th link block length |
| $K < W_\ell$ | Pilot sequence length |
| $\mathbf{e}$ | Estimation error vector |
| $\hat{\mathbf{h}} = \mathbf{h} + \mathbf{e}$ | Estimated CSI vector |
| $\mathbf{s}_\mathrm{p} = [s_{\mathrm{p}1}\, s_{\mathrm{p}2} \cdots s_{\mathrm{p}K}]^T$ | Pilot symbols vector |
| $b_{p,n}$ | $p$th relay state (on: 1 or off: 0) |
| $\mathcal{E}_{\mathbf{g}_p}\langle P_{se,\mathcal{R}_p}\rangle$ | $\mathcal{S} \to \mathcal{R}_p$ ASEP |
| $\mathcal{E}_\mathbf{h}\langle P_{se,\mathcal{D}}\vert\mathbf{b}_n\rangle$ | $\mathcal{S}, \mathcal{R}_p \to \mathcal{D}$ ASEP |
| $P_{se,e2e}$ | End-to-end ASEP |
| $\Psi_{D_\rho,D_\iota}(\jmath\omega_1, \jmath\omega_2)$ | Joint CF of $D_\rho$ and $D_\iota$ |
| $\Psi_{\|\mathbf{h}_\ell\|^2}(\jmath\omega)$ | CF of $\|\mathbf{h}_\ell\|^2 = \sum_{i=1}^{L_0} \vert h_{\ell,i}\vert^2$ |

[1]Equivalently and more generally we may assume $R+1$ orthogonal channels.

transmission energy per symbol in the $(\ell+1)$th time slot ($\ell = 0, 1, \ldots, R$) will be $\lambda_\ell\, E_\mathrm{s}$, with $\lambda_\ell \in (0,1)$ being the source ($\ell = 0$) or the $\ell$th ($\ell \neq 0$) relay to total transmission power ratio and $\sum_{\ell=0}^{R} \lambda_\ell = 1$. The $L_p \times 1$ sampled baseband complex signal vector received at relay $\mathcal{R}_p$ from $\mathcal{S}$ in the first time slot is given by

$$\mathbf{w}_p = s\,\sqrt{\lambda_0\, E_\mathrm{s}}\,\mathbf{g}_p + \boldsymbol{\nu}_p\,. \tag{1a}$$

In (1a) $\boldsymbol{\nu}_p \in \mathbb{C}^{L_p}$ is the additive white Gaussian noise (AWGN) vector, distributed as $\boldsymbol{\nu}_p \sim \mathcal{CN}\left(\mathbf{0}_{L_p}, N_0\,\mathbf{I}_{L_p}\right)$. Also, $\mathbf{g}_p = [g_{p,1}\, g_{p,2} \cdots g_{p,L_p}]^T$ stands for a random channel complex gain vector and is independent of $\boldsymbol{\nu}_p$. The elements of the Hermitian covariance matrix of $\mathbf{g}_p \in \mathbb{C}^{L_p}$ are $\mathbf{K}_{g_p}[i,j] = \mathcal{E}_{g_{p,i},g_{p,j}}\langle g_{p,i}\, g^*_{p,j}\rangle - \mathcal{E}_{g_{p,i}}\langle g_{p,i}\rangle\, \mathcal{E}^*_{g_{p,j}}\langle g_{p,j}\rangle = \varrho_{p,i,j}\,\sqrt{\Theta_{p,i}\,\Theta_{p,j}}$ for $i \neq j$, with $\varrho_{p,i,j}$ standing for the correlation coefficient between $i$th and $j$th channels ($i, j = 1, 2, \ldots, L_p$) and $\mathcal{E}_{g_{p,i}}\langle |g_{p,i}|^2\rangle = \Theta_{p,i}$ for the power of the $i$th channel between the source and the $p$th relay. Moreover, the $L_0 \times 1$ sampled baseband complex signal vector received at node $\mathcal{D}$ from $\mathcal{S}$ in the first time slot ($\ell = 0$) or from $\mathcal{R}_\ell$ in the $(\ell+1)$th time slot ($\ell \neq 0$) can be expressed as

$$\mathbf{r}_\ell = s\,\sqrt{\lambda_\ell\, E_\mathrm{s}}\,\mathbf{h}_\ell + \mathbf{n}_\ell\,. \tag{1b}$$

In (1b) $\mathbf{n}_\ell \in \mathbb{C}^{L_0}$ is the AWGN vector, distributed as $\mathbf{n}_\ell \sim \mathcal{CN}\left(\mathbf{0}_{L_0}, N_0\,\mathbf{I}_{L_0}\right)$. Also, $\mathbf{h}_\ell = [h_{\ell,1}\, h_{\ell,2} \cdots h_{\ell,L_0}]^T$ stands for a random channel complex gain vector and is independent of $\mathbf{n}_\ell$. The elements of the Hermitian covariance matrix of $\mathbf{h}_\ell \in \mathbb{C}^{L_0}$ are $\mathbf{K}_{h_\ell}[i,j] = \mathcal{E}_{h_{\ell,i},h_{\ell,j}}\langle h_{\ell,i}\, h^*_{\ell,j}\rangle - \mathcal{E}_{h_{\ell,i}}\langle h_{\ell,i}\rangle\, \mathcal{E}^*_{h_{\ell,j}}\langle h_{\ell,j}\rangle = \rho_{\ell,i,j}\,\sqrt{\Omega_{\ell,i}\,\Omega_{\ell,j}}$ for $i \neq j$, with $\rho_{\ell,i,j}$ standing for the correlation coefficient between $i$th and $j$th channels ($i, j = 1, 2, \ldots, L_0$) and $\mathcal{E}_{h_{\ell,i}}\langle |h_{\ell,i}|^2\rangle = \Omega_{\ell,i}$ for the power of the $i$th channel between the $\ell$th node and the destination.

After the first time slot, each relay performs MRC using the antennas that is equipped with. Also, after $R+1$ time slots, node $\mathcal{D}$ performs MRC with $L_0 \times$(1+number of relays that are on) signals. Due to the similarity between (1a) and (1b), next, we continue our analysis based on (1b) which is more general. Then, it shall be straightforward to transform the derived results to equivalent formulas for the $p$th source to relay link with respect to (1a). We now define three new vectors $\mathbf{r} = [\mathbf{r}_0\ \mathbf{r}_1\ \mathbf{r}_2 \cdots \mathbf{r}_R]^T$, $\mathbf{h} = [\mathbf{h}_0\ \mathbf{h}_1\ \mathbf{h}_2\ \cdots \mathbf{h}_R]^T$, and $\mathbf{n} = [\mathbf{n}_0\ \mathbf{n}_1\ \mathbf{n}_2 \cdots \mathbf{n}_R]^T$. The concatenated received signal vector at node $\mathcal{D}$ after $R+1$ time slots is

$$\mathbf{r} = s\,\sqrt{E_\mathrm{s}}\,\mathbf{V}\,\mathbf{h} + \mathbf{n}\,, \tag{2}$$

where the vector $\mathbf{h}$ is of length $L_0\,(R+1)$, with mean vector and covariance matrix $\boldsymbol{\mu}_\mathbf{h} = [\boldsymbol{\mu}_{h_0}\, \boldsymbol{\mu}_{h_1}\, \boldsymbol{\mu}_{h_2} \cdots \boldsymbol{\mu}_{h_R}]^T$ and $\mathbf{K}_\mathbf{h} = \mathrm{Diag}\{\mathbf{K}_{h_0},\ \mathbf{K}_{h_1},\ \mathbf{K}_{h_2}, \ldots, \mathbf{K}_{h_R}\}$, respectively. In (2), $\mathbf{n}$ is the noise vector $\mathbf{n} \sim \mathcal{CN}\left(\mathbf{0}_{L_0\,(R+1)}, N_0\,\mathbf{I}_{L_0\,(R+1)}\right)$ and $\mathbf{V} \in \mathbb{R}^{L_0\,(R+1)\times L_0\,(R+1)}$ is a diagonal square matrix defined as $\mathbf{V} = \mathrm{Diag}\{\sqrt{\lambda_0},\ \sqrt{\lambda_1}, \ldots, \sqrt{\lambda_R}\} \otimes \mathbf{I}_{L_0}$.

### B. Least-Squares Channel Estimation

We shall assume slowly varying block fading channels. The length of a block is closely related to the channel coherence time. In every channel block a sequence of $K$ pilot symbols is transmitted periodically. Let $\mathbf{s}_\mathrm{p} = [s_{\mathrm{p}_1}\, s_{\mathrm{p}_2} \cdots s_{\mathrm{p}_K}]^T$ be the pilot symbols vector, that is known to all relays and the destination node prior to data transmission (transmission of $s$ in (2)). Then, the CSI $\mathbf{h}$ per block is estimated based on the LSE technique after $(R+1)\,K$ time slots.

According to (2), in the $k\,(R+1)$th time slot ($k = 1, 2, \ldots, K$), the concatenated received signal vector at node $\mathcal{D}$, corresponding to the $k$th pilot symbol[2] transmission, can be expressed as

$$\mathbf{r}_{\mathrm{p}_k} = s_{\mathrm{p}_k}\,\sqrt{E_\mathrm{p}}\,\mathbf{V}\,\mathbf{h} + \mathbf{n}_{\mathrm{p}_k}\,, \tag{3}$$

where $\mathbf{n}_{\mathrm{p}_k} \sim \mathcal{CN}\left(\mathbf{0}_{L_0\,(R+1)}, N_0\,\mathbf{I}_{L_0\,(R+1)}\right)$ is the $k$th pilot AWGN concatenated vector and $E_\mathrm{p}$ is the total pilot symbols energy transmitted during $R+1$ time slots. Let $\mathbf{r}_\mathrm{p} = [\mathbf{r}_{\mathrm{p}_1}\, \mathbf{r}_{\mathrm{p}_2} \cdots \mathbf{r}_{\mathrm{p}_K}]^T$ and $\mathbf{n}_\mathrm{p} = [\mathbf{n}_{\mathrm{p}_1}\, \mathbf{n}_{\mathrm{p}_2} \cdots \mathbf{n}_{\mathrm{p}_K}]^T$ represent the concatenated received signal and AWGN vectors over $K$ pilot transmissions, respectively. Then using (3), the concatenated received pilot symbols vector at node $\mathcal{D}$ after $R+1$ time slots, $\mathbf{r}_\mathrm{p} \in \mathbb{C}^{L_0\,(R+1)\,K}$, can be written as

$$\mathbf{r}_\mathrm{p} = \sqrt{E_\mathrm{p}}\,\left(\mathbf{s}_\mathrm{p} \otimes \mathbf{I}_{L_0\,(R+1)}\right)\,\mathbf{V}\,\mathbf{h} + \mathbf{n}_\mathrm{p}\,. \tag{4}$$

From (4), the estimated CSI vector $\hat{\mathbf{h}} \in \mathbb{C}^{L_0\,(R+1)}$ by node $\mathcal{D}$ can be extracted as

$$\hat{\mathbf{h}} = \frac{1}{\sqrt{E_\mathrm{p}}\,K}\,\mathbf{V}^{-1}\,\left(\mathbf{s}_\mathrm{p}^H \otimes \mathbf{I}_{L_0\,(R+1)}\right)\,\mathbf{r}_\mathrm{p}\,. \tag{5}$$

By substituting (4) in the above equation yields

$$\hat{\mathbf{h}} = \mathbf{h} + \mathbf{e}\,, \tag{6a}$$

where

$$\mathbf{e} = \frac{1}{\sqrt{E_\mathrm{p}}\,K}\,\mathbf{V}^{-1}\,\left(\mathbf{s}_\mathrm{p}^H \otimes \mathbf{I}_{L_0\,(R+1)}\right)\,\mathbf{n}_\mathrm{p} \tag{6b}$$

is the estimation error vector and is independent of $\mathbf{h}$. Vector $\mathbf{e}$ is distributed as $\mathcal{CN}\left(\mathbf{0}_{L_0\,(R+1)}, \gamma_\mathrm{p}^{-1}\,\mathbf{V}^{-2}\right)$, with $\gamma_\mathrm{p} = K\,E_\mathrm{p}/N_0$ being the average pilot-to-noise ratio (PNR) per pilot sequence and per time slot and $N_0$ being the single-side noise power spectral density. In (6a), the mean vector and the covariance matrix of $\hat{\mathbf{h}}$ are $\boldsymbol{\mu}_{\hat{\mathbf{h}}} = \boldsymbol{\mu}_\mathbf{h}$ and $\mathbf{K}_{\hat{\mathbf{h}}} = \mathrm{Diag}\{\mathbf{K}_{h_0} + \frac{1}{\lambda_0\,\gamma_\mathrm{p}}\,\mathbf{I}_{L_0},\ \mathbf{K}_{h_1} + \frac{1}{\lambda_1\,\gamma_\mathrm{p}}\,\mathbf{I}_{L_0}, \ldots, \mathbf{K}_{h_R} + \frac{1}{\lambda_R\,\gamma_\mathrm{p}}\,\mathbf{I}_{L_0}\}$, respectively.

### C. Nakagami Fading Channel Model

A well-known and yet generic model for the complex channel gains, $h_{\ell,i}$'s (and $g_{p,i}$'s), is the Nakagami [22]. According to this model, the squared fading envelope, $|h_{\ell,i}|^2$, follows the chi-squared distribution. For not necessarily independent and identical Nakagami fading channels, the CF of $\|\mathbf{h}_\ell\|^2 = \sum_{i=1}^{L_0} |h_{\ell,i}|^2$ is given by [23]

$$\begin{aligned}\Psi_{\|\mathbf{h}_\ell\|^2}(\jmath\,\omega) &= \mathrm{Det}\left(\mathbf{I}_{L_0} - \frac{\jmath\,\omega}{m_\ell}\,\mathbf{K}_{h_\ell}\right)^{-m_\ell} \\ &= \prod_{i=1}^{N_\ell}\left(1 - \jmath\,\omega\,\frac{\epsilon_{i,\ell}}{m_\ell}\right)^{-m_\ell\,q_{i,\ell}}\,,\end{aligned} \tag{7}$$

where $m_\ell \geq 0.5$ is the Nakagami fading parameter and $\mathrm{Tr}\{\mathcal{E}\langle \mathbf{h}_\ell\,\mathbf{h}_\ell^H\rangle\} = \mathcal{E}\langle\|\mathbf{h}_\ell\|^2\rangle = \sum_{i=1}^{L_0}\Omega_{\ell,i}$. Moreover, $\epsilon_{i,\ell}$'s denote $N_\ell$ distinct eigenvalues of the covariance matrix $\mathbf{K}_{h_\ell}$ having multiplicities $q_{i,\ell}$ ($i = 1, 2, \ldots, N_\ell$), with $\sum_{i=1}^{N_\ell} q_{i,\ell} =$

[2]Our study can be also performed assuming $K$ pilots symbols with not necessarily equal powers per transmitted sequence.

TABLE II
NAKAGAMI MODEL PARAMETERS

| Symbol | Description |
|---|---|
| $m_\ell \geq 0.5$ and $\kappa_p \geq 0.5$ | Fading parameters of $\mathbf{h}_\ell$ and $\mathbf{g}_p$ |
| $\Theta_{p,i} = \mathcal{E}\langle\lvert g_{p,i}\rvert^2\rangle$ | Average power of $i$th channel of $p$th link |
| $\Omega_{\ell,i} = \mathcal{E}\langle\lvert h_{\ell,i}\rvert^2\rangle$ | Average power of $i$th channel of $\ell$th link |
| $\epsilon_{i,\ell} > 0$ and $\varepsilon_{i,p} > 0$ | Eigenvalues of $\mathbf{K}_{h_\ell}$ and $\mathbf{K}_{g_p}$ |
| $q_{i,\ell} \leq L_0$ and $\upsilon_{i,p} \leq L_p$ | Multiplicities of $\epsilon_{i,\ell}$ and $\varepsilon_{i,p}$ |
| $N_\ell \leq L_0$ and $\mathcal{N}_p \leq L_p$ | Distinct eigenvalues of $\mathbf{K}_{h_\ell}$ and $\mathbf{K}_{g_p}$ |

$L_0$ and $\sum_{i=1}^{N_\ell} q_{i,\ell}\,\epsilon_{i,\ell} = \sum_{i=1}^{L_0} \Omega_{\ell,i}$, while owing to the positive definiteness of matrix $\mathbf{K}_{h_\ell}$, $\epsilon_{i,\ell}$'s are real and positive. A summary of the Nakagami model parameters for $\mathbf{h}_\ell$ (as well as for $\mathbf{g}_p$) can be found in Table II.

## III. END-TO-END $M$-PSK AVERAGE SYMBOL ERROR PROBABILITY ANALYSIS

The on or off state for each one of the $R$ relays can be represented by a binary variable $b_{p,n}$. When the $p$th relay correctly decodes the received signal, $b_{p,n} = 1$, otherwise, $b_{p,n} = 0$. Regarding the set of binary states of all $R$ relays in the network, there are $2^R$ different combinations that can be represented by a binary vector $\mathbf{b}_n = [b_{1,n}\, b_{2,n} \cdots b_{R,n}]$, with $n = 0, 1, \ldots, 2^R - 1$. Under this notation, $\mathbf{b}_0 = \mathbf{0}_R$ when all relays are off, while $\mathbf{b}_{2^R-1} = \mathbf{1}_R$ when all relays are on.

Following the approach presented in [24], the e2e ASEP can be expressed as a sum of the average probabilities of symbol errors over all different network states, i.e.,

$$P_{se,e2e} = \sum_{n=0}^{2^R-1} \mathcal{E}_{\mathbf{h}}\left\langle P_{se,\mathcal{D}}|\mathbf{b}_n\right\rangle \prod_{p=1}^{R} \Pr\{\mathcal{R}_p :\ \text{on/off}|b_{p,n}\}\,, \tag{8}$$

where $\mathcal{E}_{\mathbf{h}}\langle P_{se,\mathcal{D}}|\mathbf{b}_n\rangle$ denotes the ASEP at node $\mathcal{D}$ (averaged on $\mathbf{h}$), with cooperation of those relays that according to $\mathbf{b}_n$ are on. Note that this probability is based on (1b). Moreover, $\Pr\{\mathcal{R}_p :\ \text{on/off}|b_{p,n}\}$ is the probability that the $p$th relay is on or off according to $b_{p,n}$. This probability is

$$\Pr\{\mathcal{R}_p :\ \text{on/off}|b_{p,n}\} = \begin{cases} \mathcal{E}_{\mathbf{g}_p}\left\langle P_{se,\mathcal{R}_p}\right\rangle, & \text{if } b_{p,n} = 0 \\ 1 - \mathcal{E}_{\mathbf{g}_p}\left\langle P_{se,\mathcal{R}_p}\right\rangle, & \text{if } b_{p,n} = 1\,, \end{cases} \tag{9}$$

with $\mathcal{E}_{\mathbf{g}_p}\langle P_{se,\mathcal{R}_p}\rangle$ being the ASEP (averaged on $\mathbf{g}_p$) for the $\mathcal{S} \to \mathcal{R}_p$ link. Note that this probability is based on (1a). Next, we focus on the derivation of $\mathcal{E}_{\mathbf{h}}\langle P_{se,\mathcal{D}}|\mathbf{b}_n\rangle$. It shall become obvious in Section III-E that $\mathcal{E}_{\mathbf{h}}\langle P_{se,\mathcal{D}}|\mathbf{b}_n\rangle$ can be efficiently used to extract $\mathcal{E}_{\mathbf{g}_p}\langle P_{se,\mathcal{R}_p}\rangle$ for the $\mathcal{S} \to \mathcal{R}_p$ link.

### A. Coherent Detection

The reception of $K$ pilot symbols per channel block transmitted by the $R+1$ nodes is followed by symbol-by-symbol reception and coherent detection of data in the destination node. For a transmitted data symbol $s$ in a symbol interval, the signals received over $L_0\,(R+1)$ diversity branches, as given by vector $\mathbf{r}$ in (2), are combined using MRC. Assuming that the network is in state $\mathbf{b}_n$, the combiner output will be $\hat{\mathbf{h}}^H \boldsymbol{B}_n\,\mathbf{r}$, where $\boldsymbol{B}_n = \text{Diag}\{b_{0,n}, b_{1,n}, \ldots, b_{R,n}\}$, with $b_{0,n}$ being a dummy variable indicating that $\mathcal{S}$ is always on, i.e., $b_{0,n} = 1$, $\forall n$. From this output, the detected symbol $\hat{s}$ is obtained as

$$\hat{s} = \arg\left\{\max_{s\in S}\ \Re\left(s^*\,\hat{\mathbf{h}}^H\,\boldsymbol{B}_n\,\mathbf{r}\right)\right\}. \tag{10}$$

When the $M$-PSK symbol $S_l$ is transmitted, the combiner output can be expressed using (2) and (6a) as

$$\begin{aligned}\hat{\mathbf{h}}^H\,\boldsymbol{B}_n\,\mathbf{r}\Big|_{s=S_l} &= \sqrt{E_\text{s}}\ (\mathbf{h}+\mathbf{e})^H\ \boldsymbol{B}_n\ (S_l\,\mathbf{V}\,\mathbf{h}+\mathbf{u}) \\ &= \sqrt{E_\text{s}}\,\tilde{D}\,,\end{aligned} \tag{11}$$

where $\tilde{D} = (\mathbf{h}+\mathbf{e})^H\,\boldsymbol{B}_n\,(S_l\,\mathbf{V}\,\mathbf{h}+\mathbf{u})$ and $\mathbf{u} = \mathbf{n}/\sqrt{E_\text{s}}$. The complex random vector $\mathbf{u}$ is independent of $\mathbf{e}$ and is distributed as $\mathbf{u} \sim \mathcal{CN}(\mathbf{0}_{L_0\,(R+1)}, \gamma^{-1}\,\mathbf{I}_{L_0\,(R+1)})$, with $\gamma = E_\text{s}/N_0$ being the total average SNR per branch and per symbol. Based on (11) and in order to be able to also consider rotated $M$-PSK constellations, we define $D = \tilde{D}\,\exp\{\jmath\,\phi\}$ as a fixed $\phi$-rad rotated combiner output. In fact,

$$D = (\mathbf{h}+\mathbf{e})^H\ \boldsymbol{B}_n\,(S_\ell\,\mathbf{V}\,\mathbf{h}\,\exp\{\jmath\,\phi\} + \mathbf{u}\,\exp\{\jmath\,\phi\}) \tag{12a}$$

is in the form of an inner product, of which we are especially interested in obtaining its statistics with respect to $\mathbf{h}$, $\mathbf{e}$ and $\mathbf{u}$. In order this to be accomplished, we first split $D$ in its real $D_\rho = \Re(D)$ and imaginary $D_\iota = \Im(D)$ parts, i.e.,

$$D = D_\rho + \jmath\,D_\iota\,, \tag{12b}$$

while next we present a useful theorem for the joint statistics of $D_\rho$ and $D_\iota$.

### B. Inner Product of Two Complex Gaussian Vectors

A new theorem is introduced as follows.

*Theorem 1 (Inner Product of Complex Gaussian Vectors: $\mathbf{Q}$ Complex)* Let $\mathbf{x} = [x_1\, x_2 \cdots x_L]^T$ and $\mathbf{y} = [y_1\, y_2 \cdots y_L]^T$ be two mutually independent complex Gaussian random vectors distributed as $\mathbf{x} \sim \mathcal{CN}(\boldsymbol{\mu}_\mathbf{x}, \mathbf{K}_\mathbf{x})$ and $\mathbf{y} \sim \mathcal{CN}(\boldsymbol{\mu}_\mathbf{y}, \mathbf{K}_\mathbf{y})$, respectively, where $\boldsymbol{\mu}_\mathbf{x} = \mathcal{E}_\mathbf{x}\langle\mathbf{x}\rangle = [\mu_{x_1}\,\mu_{x_2}\cdots\mu_{x_L}]^T$, $\mathbf{K}_\mathbf{x} = \text{Diag}\{\sigma^2_{x_1}, \sigma^2_{x_2}, \ldots, \sigma^2_{x_L}\}$ and $\boldsymbol{\mu}_\mathbf{y} = \mathcal{E}_\mathbf{y}\langle\mathbf{y}\rangle = [\mu_{y_1}\,\mu_{y_2}\cdots\mu_{y_L}]^T$, $\mathbf{K}_\mathbf{y} = \text{Diag}\{\sigma^2_{y_1}, \sigma^2_{y_2}, \ldots, \sigma^2_{y_L}\}$, with $\sigma^2_{x_i} = \mathcal{E}_{x_i}\left\langle\lvert x_i\rvert^2\right\rangle - \mathcal{E}^2_{x_i}\left\langle\lvert x_i\rvert\right\rangle$, $\sigma^2_{y_i} = \mathcal{E}_{y_i}\left\langle\lvert y_i\rvert^2\right\rangle - \mathcal{E}^2_{y_i}\left\langle\lvert y_i\rvert\right\rangle$ $\forall i = 1, 2, \ldots, L$. Also let the complex random variable (rv) $z \in \mathbb{C}$ be given by the inner product of $\mathbf{y}$ and $\mathbf{Q}\,\mathbf{x}$, i.e.,

$$z = \mathbf{y}^H\,\mathbf{Q}\,\mathbf{x} = z_\rho + \jmath\,z_\iota\,, \tag{13}$$

with $z_\rho = \Re\{z\}$, $z_\iota = \Im\{z\}$, and $\mathbf{Q} = \text{Diag}\{q_1, q_2, \ldots, q_L\}$ being a square diagonal matrix, $\mathbf{Q} \in \mathbb{C}^{L\times L}$. Then, the joint CF of $z_\rho$ and $z_\iota$ is given by (14) (at the top of the next page).

The proof of Theorem 1 is given in the Appendix A. Note that [8, eq. (2)] is a special case of (14) for $\mathbf{Q} = \mathbf{I}_L$, $\mathbf{K}_\mathbf{x} = \sigma^2_x\,\mathbf{I}_L$, and $\mathbf{K}_\mathbf{y} = \sigma^2_y\,\mathbf{I}_L$. Since $\boldsymbol{B}_n$ in (12a) is a square matrix with binary elements, we present the following corollary.

*Corollary 1 (Inner Product of Complex Gaussian Vectors: $\mathbf{Q}$ Binary)* Let $\mathbf{Q}$ be a diagonal matrix with binary $q_i$'s and $z$, $\mathbf{x}$ and $\mathbf{y}$ defined as in Theorem 1. Then, the joint CF of $z_\rho$ and $z_\iota$ is given by (15) (at the top of the next page).

It is straightforward to extract (15) from (14) when $q_i$'s are binary. Therefore, the proof of the above corollary is omitted.

### C. Joint CF of Real and Imaginary Parts of MRC Output

By comparing (12a) with (13), we can easily conclude that they are of the same form. Specifically, conditioned on $\mathbf{h}$, the two vectors consisting the inner product in (12a), i.e., $\mathbf{y} = \mathbf{h}+\mathbf{e}$ and $\mathbf{x} = S_l\,\mathbf{V}\,\mathbf{h}\,\exp\{\jmath\,\phi\} + \mathbf{u}\,\exp\{\jmath\,\phi\}$, are complex Gaussian and mutually independent, with $\mathbf{y} \sim \mathcal{CN}(\mathbf{h}, \gamma_\text{p}^{-1}\,\mathbf{V}^{-2})$ and

$$\Psi_{z_\rho,z_\iota}(\jmath\omega_1,\jmath\omega_2)=\prod_{i=1}^{L}\left(1+\frac{\omega_1^2+\omega_2^2}{4}\,|q_i|^2\sigma_{x_i}^2\,\sigma_{y_i}^2\right)^{-1} \times\exp\left\{-\frac{\frac{\omega_1^2+\omega_2^2}{4}\,|q_i|^2\left(|\mu_{x_i}|^2\,\sigma_{y_i}^2+|\mu_{y_i}|^2\,\sigma_{x_i}^2\right)-\jmath\,\Re\left\{(\omega_1-\jmath\,\omega_2)\,\mu_{y_i}^*\,q_i\,\mu_{x_i}\right\}}{1+\frac{\omega_1^2+\omega_2^2}{4}\,|q_i|^2\,\sigma_{x_i}^2\,\sigma_{y_i}^2}\right\} \tag{14}$$

$$\Psi_{z_\rho,z_\iota}(\jmath\omega_1,\jmath\omega_2)=\prod_{i=1}^{L}\left(1+\frac{\omega_1^2+\omega_2^2}{4}\,\sigma_{x_i}^2\,\sigma_{y_i}^2\right)^{-q_i} \times\exp\left\{-q_i\,\frac{\frac{\omega_1^2+\omega_2^2}{4}\left(|\mu_{x_i}|^2\,\sigma_{y_i}^2+|\mu_{y_i}|^2\,\sigma_{x_i}^2\right)-\jmath\,\Re\left\{(\omega_1-\jmath\,\omega_2)\,\mu_{y_i}^*\,\mu_{x_i}\right\}}{1+\frac{\omega_1^2+\omega_2^2}{4}\,\sigma_{x_i}^2\,\sigma_{y_i}^2}\right\} \tag{15}$$

$$\begin{aligned}\Psi_{D_\rho,D_\iota|\mathbf{h}}(\jmath\omega_1,\jmath\omega_2|\mathbf{h})&=\mathcal{E}_{D_\rho,D_\iota|\mathbf{h}}\left\langle\exp\left\{\jmath\left(\omega_1\,D_\rho+\omega_2\,D_\iota\right)\right\}\middle|\,\mathbf{h}\right\rangle\\&=\prod_{\ell=0}^{R}\exp\left\{-b_{\ell,n}\,\frac{\left(\omega_1^2+\omega_2^2\right)\,\frac{\gamma+\gamma_\mathrm{p}}{4\,\gamma\,\gamma_\mathrm{p}}-\jmath\,\sqrt{\lambda_\ell}\left(\omega_1\,\Re\{e^{\jmath\,\phi}\}+\omega_2\,\Im\{e^{\jmath\,\phi}\}\right)}{1+\frac{\omega_1^2+\omega_2^2}{4\,\lambda_\ell\,\gamma\,\gamma_\mathrm{p}}}\,\|\mathbf{h}_\ell\|^2\right\}\left(1+\frac{\omega_1^2+\omega_2^2}{4\,\lambda_\ell\,\gamma\,\gamma_\mathrm{p}}\right)^{-b_{\ell,n}\,L_0}\end{aligned} \tag{16}$$

$$\Psi_{D_\rho,D_\iota}(\jmath\omega_1,\jmath\omega_2)=\prod_{\ell=0}^{R}\Psi_{\|\mathbf{h}_\ell\|^2}^{b_{\ell,n}}\left\{-\frac{\left(\omega_1^2+\omega_2^2\right)\,\frac{\gamma+\gamma_\mathrm{p}}{4\,\gamma\,\gamma_\mathrm{p}}-\jmath\,\sqrt{\lambda_\ell}\left(\omega_1\,\Re\{e^{\jmath\,\phi}\}+\omega_2\,\Im\{e^{\jmath\,\phi}\}\right)}{1+\frac{\omega_1^2+\omega_2^2}{4\,\lambda_\ell\,\gamma\,\gamma_\mathrm{p}}}\right\}\left(1+\frac{\omega_1^2+\omega_2^2}{4\,\lambda_\ell\,\gamma\,\gamma_\mathrm{p}}\right)^{-b_{\ell,n}\,L_0} \tag{17}$$

$$\Psi_{D_\rho,D_\iota}(\jmath\omega_1,\jmath\omega_2)=\prod_{\ell=0}^{R}\frac{\left(1+\frac{\omega_1^2+\omega_2^2}{4\,\lambda_\ell\,\gamma\,\gamma_\mathrm{p}}\right)^{b_{\ell,n}\,(m_\ell-1)\,L_0}}{\prod_{k=1}^{N_\ell}\left(1-\jmath\,\frac{\epsilon_{k,\ell}}{m_\ell}\,\sqrt{\lambda_\ell}\,\left(\omega_1\,\Re\{e^{\jmath\,\phi}\}+\omega_2\,\Im\{e^{-\jmath\,\phi}\}\right)+\left(\omega_1^2+\omega_2^2\right)\,\frac{(\gamma+\gamma_\mathrm{p})\epsilon_{k,\ell}/m_\ell+1/\lambda_\ell}{4\,\gamma\,\gamma_\mathrm{p}}\right)^{b_{\ell,n}\,m_\ell\,q_{k,\ell}}} \tag{18}$$

$\mathbf{x}\sim\mathcal{CN}(S_l\,\mathbf{V}\,\mathbf{h},\gamma^{-1}\,\mathbf{I}_{L_0\,(R+1)})$. By applying the Corollary 1 in (12a), the joint CF of $D_\rho$ and $D_\iota$, conditioned on $\mathbf{h}$, is given by (16) (at top of this page). By averaging (16) over $\mathbf{h}$, i.e., $\mathcal{E}_\mathbf{h}\langle\Psi_{D_\rho,D_\iota|\mathbf{h}}(\jmath\omega_1,\jmath\omega_2|\mathbf{h})\rangle=\Psi_{D_\rho,D_\iota}(\jmath\omega_1,\jmath\omega_2)$ and by the definition of the CF of $\|\mathbf{h}_\ell\|^2$, the joint CF of $D_\rho$ and $D_\iota$ yields as in (17) (at top of this page). Note that (17) is a quite general expression in the sense that it only requires a readily available expression for the CF of the sum of squared fading envelopes for the distribution under consideration.

Now by assuming Nakagami fading and by substituting (7) in (17), the joint CF of $D_\rho$ and $D_\iota$ is obtained as in (18) (at top of this page).

### D. $M$-PSK ASEP Expressions for $\mathcal{E}_\mathbf{h}\langle P_{se,\mathcal{D}}|\mathbf{b}_n\rangle$

Based on (17), next, we provide general ASEP expressions for $\mathcal{E}_\mathbf{h}\langle P_{se,\mathcal{D}}|\mathbf{b}_n\rangle$, assuming $M$-PSK PSAM, with cooperation of those relays that according to $\mathbf{b}_n$ are on. All these expressions can be easily evaluated via numerical integration. Furthermore, based on (18), we provide corresponding analytical expressions for Nakagami fading.

*1) BPSK:* For $M=2$ we assume that $S_0$ is transmitted with $\phi=0$. The ABEP of pilot-symbol assisted BPSK can be obtained as

$$\mathcal{E}_\mathbf{h}\left\langle P_{be,\mathcal{D}}|\mathbf{b}_n\right\rangle=\Pr\{D_\rho<0\}\,. \tag{19}$$

The probability in (19) can be directly evaluated using the Gil-Pelaez inversion theorem [25] as

$$\mathcal{E}_\mathbf{h}\left\langle P_{be,\mathcal{D}}|\mathbf{b}_n\right\rangle=\frac{1}{2}-\frac{1}{2\,\pi}\int_{-\infty}^{\infty}\frac{1}{\omega}\,\Im\left\{\Psi_{D_\rho}(\jmath\omega)\right\}\mathrm{d}\omega\,, \tag{20}$$

with $\Psi_{D_\rho}(\jmath\omega)=\Psi_{D_\rho,D_\iota}(\jmath\omega,0)$ being a marginal CF of $\Psi_{D_\rho,D_\iota}(\jmath\omega_1,\jmath\omega_2)$.

For Nakagami fading, by setting $\tau=\jmath\omega_1$ and $\omega_2=0$ in (18), the moments-generating function (MGF) of $D_\rho$ can be compactly expressed as

$$\Psi_{D_\rho}(\tau)=\prod_{\ell=0}^{R}\frac{\left(1-\frac{\tau^2}{4\,\gamma\,\gamma_\mathrm{p}\,\lambda_\ell}\right)^{b_{\ell,n}\,(m_\ell-1)\,L_0}}{\prod_{k=1}^{N_\ell}\left(1-\tau\,\nu_{k\ell1}\right)^{b_{\ell,n}\,m_\ell\,q_{k,\ell}}\left(1-\tau\,\nu_{k\ell2}\right)^{b_{\ell,n}\,m_\ell\,q_{k,\ell}}}\,, \tag{21}$$

with

$$\nu_{k\ell1}=\frac{\epsilon_{k,\ell}}{2\,m_\ell}\left(\sqrt{\lambda_\ell}+\sqrt{\lambda_\ell+\frac{(\gamma+\gamma_\mathrm{p})\,\epsilon_{k,\ell}/m_\ell+1/\lambda_\ell}{\gamma\,\gamma_\mathrm{p}\,(\epsilon_{k,\ell}/m_\ell)^2}}\right) \tag{22a}$$

and

$$\nu_{k\ell2}=\frac{\epsilon_{k,\ell}}{2\,m_\ell}\left(\sqrt{\lambda_\ell}-\sqrt{\lambda_\ell+\frac{(\gamma+\gamma_\mathrm{p})\,\epsilon_{k,\ell}/m_\ell+1/\lambda_\ell}{\gamma\,\gamma_\mathrm{p}\,(\epsilon_{k,\ell}/m_\ell)^2}}\right), \tag{22b}$$

$$\mathcal{E}_{\mathbf{h}}\left\langle P_{be,\mathcal{D}}|\mathbf{b}_n\right\rangle_{\gamma\neq\gamma_{\rm p}} = \sum_{\ell=0}^{R} b_{\ell,n} \sum_{k=1}^{N_\ell} \frac{1}{(m_\ell\, q_{k,\ell}-1)!} \left[\prod_{i=0}^{R} \frac{\left(1-\frac{1}{4\,\lambda_i\,\gamma\,\gamma_{\rm p}\,\nu_{k\ell2}^2}\right)^{b_{i,n}\,(m_i-1)\,L_0}}{\left[\prod\limits_{t=1}^{N_i}\left(1-\frac{\nu_{ti1}}{\nu_{k\ell2}}\right)^{b_{i,n}\,m_i\,q_{t,\ell}}\right]\prod\limits_{\substack{t=1\\-\{t=k\wedge i=\ell\}}}^{N_i}\left(1-\frac{\nu_{ti2}}{\nu_{k\ell2}}\right)^{b_{i,n}\,m_i\,q_{t,\ell}}}\right] \times \sum_{\substack{l_1,l_2,\ldots,l_{m_\ell\,q_{k,\ell}-1}=0\\0\le l_1,\ldots,l_{m_\ell\,q_{k,\ell}-1}\le m_\ell\,q_{k,\ell}-1\\l_1+2l_2+\cdots+(m_\ell\,q_{k,\ell}-1)l_{m_\ell\,q_{k,\ell}-1}=m_\ell\,q_{k,\ell}-1}} \prod_{w=1}^{m_\ell\,q_{k,\ell}-1}\frac{w^{1-l_w}}{l_w!} \times\left\{1+\sum_{i=0}^{R} b_{i,n}\left[-(m_i-1)\,L_0\left(\left(1-2\,\nu_{k\ell2}\,\sqrt{\gamma\,\gamma_{\rm p}\,\lambda_i}\right)^{-w}+\left(1+2\,\nu_{k\ell2}\,\sqrt{\gamma\,\gamma_{\rm p}\,\lambda_i}\right)^{-w}\right)+\sum_{t=1}^{N_i} m_i\,q_{t,\ell}\left(1-\frac{\nu_{k\ell2}}{\nu_{ti1}}\right)^{-w}+\sum_{\substack{t=1\\-\{t=k\wedge i=\ell\}}}^{N_i} m_i\,q_{t,\ell}\left(1-\frac{\nu_{k\ell2}}{\nu_{ti2}}\right)^{-w}\right]\right\}^{l_w} \tag{24}$$

where $\nu_{k\ell1}>0$ and $\nu_{k\ell2}<0$, $\forall\ k=1,2,\ldots,N_\ell$ and $\ell=0,1,\ldots,R$. By substituting (21) in (20) and by applying the Cauchy's residue theorem, the ABEP of BPSK can be obtained as the negative of the sum of residues of $\Psi_{D_\rho}(\tau)/\tau$ at poles on the left-half $\tau$-plane, that are at $\tau=1/\nu_{k\ell2}\ \forall\ k$ and $\ell$. For $\gamma\neq\gamma_{\rm p}$, this sum is given by

$$\mathcal{E}_{\mathbf{h}}\left\langle P_{be,\mathcal{D}}|\mathbf{b}_n\right\rangle_{\gamma\neq\gamma_{\rm p}} = -\sum_{\ell=0}^{R} b_{\ell,n}\sum_{k=1}^{N_\ell}\mathrm{Res}\left\{\frac{\Psi_{D_\rho}(\tau)}{\tau}\right\}\Big|_{\tau=\frac{1}{\nu_{k\ell2}}}, \tag{23}$$

while after a lot of algebraic manipulations can be expressed in closed form as (24) (at top of this page). Similarly, for $\gamma=\gamma_{\rm p}$, (21) simplifies as

$$\Psi_{D_\rho}(\tau)=\prod_{\ell=0}^{R}\frac{\left(1+\tau\,\nu_{\ell2}\right)^{b_{\ell,n}\,(m_\ell-1)\,L_0}}{\left(1-\tau\,\nu_{\ell2}\right)^{b_{\ell,n}\,L_0}\prod\limits_{k=1}^{N_\ell}\left(1-\tau\,\nu_{k\ell1}\right)^{b_{\ell,n}\,m_\ell\,q_{k,\ell}}}, \tag{25}$$

with

$$\nu_{k\ell1}=\sqrt{\lambda_\ell}\,\frac{\epsilon_{k,\ell}}{m_\ell}+\frac{1}{2\,\gamma\,\sqrt{\lambda_\ell}}>0 \tag{26a}$$

and

$$\nu_{\ell2}=-\frac{1}{2\,\gamma\,\sqrt{\lambda_\ell}}<0\,, \tag{26b}$$

while the sum of residues can be written in the form

$$\mathcal{E}_{\mathbf{h}}\left\langle P_{be,\mathcal{D}}|\mathbf{b}_n\right\rangle_{\gamma=\gamma_{\rm p}} = -\sum_{\ell=0}^{R} b_{\ell,n}\,\mathrm{Res}\left\{\frac{\Psi_{D_\rho}(\tau)}{\tau}\right\}\Big|_{\tau=\frac{1}{\nu_{\ell2}}}, \tag{27}$$

yielding (28) (at top of the next page). Note that (24) and (28) consist only of elementary functions.

*2) QPSK:* For $M=4$ we consider a $\phi=\pi/4$ rotated constellation and we assume that $S_2$ is transmitted. For equiprobable symbols, the QPSK ASEP can be calculated as

$$\mathcal{E}_{\mathbf{h}}\left\langle P_{se,\mathcal{D}}|\mathbf{b}_n\right\rangle = 1-\Pr\{D_\rho\le 0, D_\iota\le 0\}\,. \tag{29}$$

The probability of the joint event $D_\rho\le 0$ and $D_\iota\le 0$ can be analytically evaluated based on the multivariate inversion theorem [26, eq. (11)] according to which yields

$$\mathcal{E}_{\mathbf{h}}\left\langle P_{se,\mathcal{D}}|\mathbf{b}_n\right\rangle = \frac{5}{4}-\frac{1}{2}\,(P_1+P_2) + \frac{1}{2\,\pi^2}\int_0^\infty\int_0^\infty \frac{1}{\omega_1\,\omega_2}\,\Re\left\{\Psi_{D_\rho,D_\iota}\left(\jmath\,\omega_1,\jmath\,\omega_2\right) -\Psi_{D_\rho,D_\iota}\left(\jmath\,\omega_1,-\jmath\,\omega_2\right)\right\}\mathrm{d}\omega_1\,\mathrm{d}\omega_2\,, \tag{30}$$

with $P_1=\Pr\{D_\rho\le 0\}$, $P_2=\Pr\{D_\iota\le 0\}$, and both can be evaluated using (20).

By substituting (18) in (30), an exact analytical $M$-PSK ASEP expression can be obtained for correlated Nakagami fading.

*3) $M$-PSK for High SNR:* For arbitrary $M\ge 2$ we assume that $S_0$ is transmitted with $\phi=0$. Using [8, eq. (39)] and (16), we get the ASEP of $M$-PSK as

$$\mathcal{E}_{\mathbf{h}}\left\langle P_{se,\mathcal{D}}|\mathbf{b}_n\right\rangle = \frac{1}{4\,\pi^2} \times\int_{\rho=0}^{\infty}\int_{\theta=-\pi}^{\pi}\left(\prod_{\ell=0}^{R}\frac{\Psi_{\|\mathbf{h}_\ell\|^2}^{b_{\ell,n}}\left\{-\frac{\rho^2\,\frac{\gamma+\gamma_{\rm p}}{4\,\gamma\,\gamma_{\rm p}}-\jmath\sqrt{\lambda_\ell}\,\rho\,\cos(\theta)}{1+\frac{\rho^2}{4\,\lambda_\ell\,\gamma\,\gamma_{\rm p}}}\right\}}{\left(1+\frac{\rho^2}{4\,\lambda_\ell\,\gamma\,\gamma_{\rm p}}\right)^{L_0\,b_{\ell,n}}}\right) \times\frac{P(\theta,M)}{\rho}\,\mathrm{d}\theta\,\mathrm{d}\rho\,, \tag{31}$$

with $P(\cdot,\cdot)$ defined in [8, eq. (38)]. Following a similar procedure such that in [8, Section IV.C], and applying [8, eq. (43)] in (31) for high SNR ($\gamma\gg 1$ and $\gamma_{\rm p}\gg 1$), an approximate ASEP expression yields

$$\mathcal{E}_{\mathbf{h}}\left\langle P_{se,\mathcal{D}}|\mathbf{b}_n\right\rangle \approx\frac{1}{\pi}\int_0^{\pi\frac{M-1}{M}}\prod_{\ell=0}^{R}\Psi_{\|\mathbf{h}_\ell\|^2}^{b_{\ell,n}}\left(-\lambda_\ell\,\frac{\gamma\,\gamma_{\rm p}}{\gamma+\gamma_{\rm p}}\,\frac{\sin^2(\pi/M)}{\sin^2(\alpha)}\right)\mathrm{d}\alpha\,. \tag{32}$$

$$\mathcal{E}_{\mathbf{h}}\left\langle P_{se,\mathcal{D}}|\mathbf{b}_n\right\rangle_{\gamma=\gamma_{\rm p}} = \sum_{\ell=0}^{R}\frac{b_{\ell,n}}{(L_0-1)!}\left[\prod_{\substack{i=0\\ i\neq\ell}}^{R}\left(1-\sqrt{\frac{\lambda_\ell}{\lambda_i}}\right)^{-b_{i,n}\,L_0}\right]\left[\prod_{i=0}^{R}\frac{\left(1+\sqrt{\frac{\lambda_\ell}{\lambda_i}}\right)^{b_{i,n}\,(m_i-1)\,L_0}}{\prod_{k=1}^{N_i}\left(1+2\,\gamma\sqrt{\lambda_\ell}\,\nu_{ik1}\right)^{b_{i,n}\,m_i\,q_{k,\ell}}}\right]\sum_{\substack{l_1,l_2,\ldots,l_{L_0-1}=0\\ 0\le l_1,\ldots,l_{L_0-1}\le L_0-1\\ l_1+2l_2+\cdots+(L_0-1)l_{L_0-1}=L_0-1}}^{L_0-1}\prod_{w=1}^{L_0-1}\frac{w^{1-l_w}}{l_w!}\left\{1+L_0\sum_{\substack{i=0\\ i\neq\ell}}^{R}b_{i,n}\left(1-\sqrt{\frac{\lambda_i}{\lambda_\ell}}\right)^{-w}-\sum_{i=0}^{R}b_{i,n}\left[\frac{(m_i-1)\,L_0}{\left(1+\sqrt{\frac{\lambda_i}{\lambda_\ell}}\right)^{w}}-\sum_{k=1}^{N_i}\frac{m_i\,q_{k,\ell}}{\left(1+\frac{1}{2\,\gamma\sqrt{\lambda_\ell}\,\nu_{ik1}}\right)^{w}}\right]\right\}^{l_w} \tag{28}$$

An upper bound for $\mathcal{E}_{\mathbf{h}}\left\langle P_{se,\mathcal{D}}|\mathbf{b}_n\right\rangle$ can be also derived setting $\sin^2(\alpha)=1$ in (32), resulting in

$$\mathcal{E}_{\mathbf{h}}\left\langle P_{se,\mathcal{D}}|\mathbf{b}_n\right\rangle \le \frac{M-1}{M}\prod_{\ell=0}^{R}\Psi_{\|\mathbf{h}_\ell\|^2}^{b_{\ell,n}}\left(-\lambda_\ell\,\frac{\gamma\,\gamma_{\rm p}}{\gamma+\gamma_{\rm p}}\,\sin^2\left(\frac{\pi}{M}\right)\right). \tag{33}$$

It can be easily verified that for a fixed value of $\gamma_{\rm p}$ and as $\gamma\to\infty$, $\mathcal{E}_{\mathbf{h}}\left\langle P_{se,\mathcal{D}}|\mathbf{b}_n\right\rangle$ tends to a constant value, i.e., we get an irreducible error floor.

Using (32) and (7) for Nakagami fading, a high-SNR ASEP expression yields

$$\mathcal{E}_{\mathbf{h}}\left\langle P_{se,\mathcal{D}}|\mathbf{b}_n\right\rangle \approx \frac{1}{\pi}\int_0^{\pi\frac{M-1}{M}}\prod_{\ell=0}^{R}\prod_{i=1}^{N_\ell}\left(1+\lambda_\ell\,\frac{\gamma\,\gamma_{\rm p}}{\gamma+\gamma_{\rm p}}\times\frac{\epsilon_{i,\ell}}{m_\ell}\,\frac{\sin^2(\pi/M)}{\sin^2(\alpha)}\right)^{-b_{\ell,n}\,m_\ell\,q_{i,\ell}}\mathrm{d}\alpha\,. \tag{34}$$

Although (34) can be easily evaluated using numerical integration techniques, some insights of $\mathcal{E}_{\mathbf{h}}\langle P_{se,\mathcal{D}}|\mathbf{b}_n\rangle$ can be revealed as follows. For (34), it can be easily proved that

$$\begin{aligned} I_\zeta &= \lim_{\forall i,\ell,\ x_{i,\ell}\to\infty}\left(\prod_{\ell=0}^{R}\prod_{i=1}^{N_\ell}x_{i,\ell}^{b_{\ell,n}\,m_\ell\,q_{i,\ell}}\right)\mathcal{E}_{\mathbf{h}}\left\langle P_{se,\mathcal{D}}|\mathbf{b}_n\right\rangle \\ &= \frac{1}{\pi}\left(\frac{\sqrt{\pi}}{2}\,\frac{\Gamma\left(\frac{1}{2}+\zeta\right)}{\Gamma\left(1+\zeta\right)}-\xi\,{}_2F_1\left(\frac{1}{2},\frac{1}{2}-\zeta;\frac{3}{2};\xi^2\right)\right), \end{aligned} \tag{35}$$

with $x_{i,\ell}=G\,\lambda_\ell\,\frac{\epsilon_{i,\ell}}{m_\ell}$, $G=\frac{\gamma\,\gamma_{\rm p}}{\gamma+\gamma_{\rm p}}\,\sin^2(\frac{\pi}{M})$, $\xi=\cos(\pi\,\frac{M-1}{M})$, $\zeta=L_0\,\sum_{\ell=0}^{R}b_{\ell,n}\,m_\ell$, and with $\Gamma(\cdot)$ and ${}_2F_1(\cdot,\cdot;\cdot;\cdot)$ being the Gamma and Gauss hypergeometric functions, respectively. Using (34) and (35), an alternative closed-form expression for $\mathcal{E}_{\mathbf{h}}\left\langle P_{se,\mathcal{D}}|\mathbf{b}_n\right\rangle$ can be obtained as

$$\mathcal{E}_{\mathbf{h}}\left\langle P_{se,\mathcal{D}}|\mathbf{b}_n\right\rangle = I_\zeta\,G^{-\zeta}\prod_{\ell=0}^{R}\frac{\lambda_\ell^{-b_{\ell,n}\,m_\ell\,L_0}}{\prod_{i=1}^{N_\ell}\left(\epsilon_{i,\ell}/m_\ell\right)^{b_{\ell,n}\,m_\ell\,q_{i,\ell}}}. \tag{36}$$

The above expression is quite useful because it includes $G$ and $\lambda_\ell$'s as separate power product terms. This specific form for $\mathcal{E}_{\mathbf{h}}\left\langle P_{se,\mathcal{D}}|\mathbf{b}_n\right\rangle$ simplifies the analysis for the OPA, while provides important information concerning the cooperation-gain and diversity-order.

### *E. Derivation of $\mathcal{E}_{\mathbf{g}_p}\langle P_{se,\mathcal{R}_p}\rangle$ From $\mathcal{E}_{\mathbf{h}}\langle P_{se,\mathcal{D}}|\mathbf{b}_n\rangle$*

As already mentioned in Section II-A, all the preceding analysis has been performed with respect to (1b). However, the e2e ASEP in (8) also requires the knowledge of $\mathcal{E}_{\mathbf{g}_p}\langle P_{se,\mathcal{R}_p}\rangle$ with respect to (1a). In order to be able to extract $\mathcal{E}_{\mathbf{g}_p}\langle P_{se,\mathcal{R}_p}\rangle$ from $\mathcal{E}_{\mathbf{h}}\langle P_{se,\mathcal{D}}|\mathbf{b}_n\rangle$, the substitutions of all those pairs of symbols provided in Table III should be performed. For example, using Table III with (36) yields

$$\mathcal{E}_{\mathbf{g}_p}\left\langle P_{se,\mathcal{R}_p}\right\rangle = \frac{I_{\kappa_p\,L_p}\,G^{-\kappa_p\,L_p}}{\prod_{i=1}^{\mathcal{N}_p}\left(\varepsilon_{i,p}/\kappa_p\right)^{\kappa_p\,\upsilon_{i,p}}}\,\frac{1}{\lambda_0^{\kappa_p\,L_p}}, \tag{37}$$

with $\varepsilon_{i,p}$'s and $\upsilon_{i,p}$'s being respectively $\mathcal{N}_p$ positive eigenvalues and their multiplicities of the $\mathcal{S}\to\mathcal{R}_p$ Nakagami channel and $\kappa_p\ge 0.5$ being the fading parameter.

TABLE III
SUBSTITUTION PAIRS OF SYMBOLS FOR DERIVING $\mathcal{E}_{\mathbf{g}_p}\langle P_{se,\mathcal{R}_p}\rangle$ FROM $\mathcal{E}_{\mathbf{h}}\langle P_{se,\mathcal{D}}|\mathbf{b}_n\rangle$ IN SECTIONS II-C, III-C AND III-D

| Current Formula Based on (1b) | New Formula Based on (1a) |
|---|---|
| $\mathbf{h}_\ell$ | $\mathbf{g}_p$ |
| $L_0$ | $L_p$ |
| $\lambda_\ell$ | $\lambda_0$ |
| $\sum_{\ell=0}^{R}$ or $\prod_{\ell=0}^{R}$ | – |
| $b_{\ell,n}$ | 1 |
| $m_\ell$ | $\kappa_p$ |
| $\Omega_{\ell,i}$ | $\Theta_{p,i}$ |
| $\epsilon_{i,\ell}$ | $\varepsilon_{i,p}$ |
| $q_{i,\ell}$ | $\upsilon_{i,p}$ |
| $N_\ell$ | $\mathcal{N}_p$ |
| $\nu_{k\ell1}$, $\nu_{k\ell2}$ | $\nu_{kp1}$, $\nu_{kp2}$ |

### *F. E2E $M$-PSK ASEP for High SNR*

Using (8) and Table III with any of (20), (30) or (32), general e2e ASEP expression can be derived for any fading channel model under consideration.

For Nakagami fading, by substituting (36) and (37) in (8), the e2e ASEP of $M$-PSK for high SNR can be expressed as

$$P_{se,e2e}=\sum_{n=0}^{2^R-1}\frac{I_\zeta\prod_{\ell=0}^{R}(G\,\lambda_\ell)^{-b_{\ell,n}\,m_\ell\,L_0}}{\prod_{\ell=0}^{R}\prod_{i=1}^{N_\ell}\left(\epsilon_{i,\ell}/m_\ell\right)^{b_{\ell,n}\,m_\ell\,q_{i,\ell}}}\times\prod_{p=1}^{R}\left[b_{p,n}+(-1)^{b_{p,n}}\,\frac{I_{\kappa_p\,L_p}\,(\lambda_0\,G)^{-\kappa_p\,L_p}}{\prod_{i=1}^{\mathcal{N}_p}\left(\varepsilon_{i,p}/\kappa_p\right)^{\kappa_p\,\upsilon_{i,p}}}\right] \tag{38}$$

and can be accurately approximated as

$$P_{se,e2e}\simeq\sum_{n=0}^{2^R-1}\frac{I_\zeta\prod_{\ell=0}^{R}(G\,\lambda_\ell)^{-b_{\ell,n}\,m_\ell\,L_0}}{\prod_{\ell=0}^{R}\prod_{i=1}^{N_\ell}\left(\epsilon_{i,\ell}/m_\ell\right)^{b_{\ell,n}\,m_\ell\,q_{i,\ell}}}\times\prod_{p=1}^{R}\left[\frac{I_{\kappa_p\,L_p}\,(\lambda_0\,G)^{-\kappa_p\,L_p}}{\prod_{i=1}^{\mathcal{N}_p}\left(\varepsilon_{i,p}/\kappa_p\right)^{\kappa_p\,\upsilon_{i,p}}}\right]^{1-b_{p,n}}. \tag{39}$$

## IV. Cooperation-Gain, Diversity-Order and OPA

In an effort to highlight some direct benefits of our proposed formulation, this section presents some further analysis on the e2e ASEP over Nakagami fading, including the derivation of the cooperation-gain, diversity-order, and OPA.

### A. Cooperation-Gain and Diversity-Order

When $\gamma, \gamma_{\rm p} \to \infty$, i.e., $G \to \infty$, simple e2e approximate ASEP expressions can be obtained for two meaningful limiting cases: (*i*) $L_0 > L_p$ and $m > \kappa$, (*ii*) $L_0 < L_p$ and $m < \kappa$, assuming $m_\ell = m \; \forall \ell$ and $\kappa_p = \kappa \; \forall p$. Using (39), $P_{se,e2e}$ can be expressed as

$$P_{se,e2e} \simeq \sum_{n=0}^{2^R-1} \frac{\mathcal{A}_n}{G^{m\,L_0+\sum_{p=1}^{R}[b_{p,n}\,m\,L_0+(1-b_{p,n})\,\kappa\,L_p]}}\,, \quad (40)$$

where

$$\mathcal{A}_n = \frac{I_\zeta\,\lambda_0^{-\,m\,L_0}}{\prod_{i=1}^{N_0}\left(\frac{\epsilon_{i,0}}{m}\right)^{m\,q_{i,0}}} \times \prod_{p=1}^{R} \frac{\lambda_p^{-b_{p,n}\,m\,L_0}}{\prod_{i=1}^{\mathcal{N}_p}\left(\frac{\epsilon_{i,p}}{m}\right)^{b_{p,n}\,m\,q_{i,p}}} \left[\frac{I_{\kappa\,L_p}\,\lambda_0^{-\kappa\,L_p}}{\prod_{i=1}^{\mathcal{N}_p}\left(\frac{\varepsilon_{i,p}}{\kappa}\right)^{\kappa\,\upsilon_{i,p}}}\right]^{1-b_{p,n}}.$$

The dominant term in the above sum as $G \to \infty$ will be the one that is in the lowest power of $G$. It can be easily verified that for cases (*i*) and (*ii*), these terms correspond to network states $\mathbf{b}_0$ and $\mathbf{b}_{2^R-1}$, respectively. Hence, the e2e $M$-PSK ASEPs can be simplified as

$$P_{se,e2e} \simeq \frac{I_{m\,L_0}\,(G\,\lambda_0)^{-\,m\,L_0-\kappa\sum_{p=1}^{R}L_p}}{\prod_{i=1}^{N_0}\left(\frac{\epsilon_{i,0}}{m}\right)^{m\,q_{i,0}}} \prod_{p=1}^{R} \frac{I_{\kappa\,L_p}}{\prod_{i=1}^{\mathcal{N}_p}\left(\frac{\varepsilon_{i,p}}{\kappa}\right)^{\kappa\,\upsilon_{i,p}}}\,, \quad (41a)$$

for case (*i*) and

$$P_{se,e2e} \simeq I_{m\,L_0\,(R+1)} \prod_{\ell=0}^{R} \frac{(G\,\lambda_\ell)^{-m\,L_0}}{\prod_{i=1}^{N_\ell}\left(\epsilon_{i,\ell}/m\right)^{m\,q_{i,\ell}}}\,, \quad (41b)$$

for case (*ii*). By transforming the above e2e ASEP expressions in the form $P_{se,e2e} = \lim_{\gamma\to\infty} (\mathcal{G}_c/\gamma)^{\mathcal{G}_d}$, the cooperation-gain, $\mathcal{G}_c$, and diversity-order, $\mathcal{G}_d$, can be obtained as follows. From (41a), when $\gamma_{\rm p} \to \infty$, i.e., $G \simeq \gamma \sin^{-2}(\pi/M)$, $\mathcal{G}_c$ and $\mathcal{G}_d$ are given by

$$\mathcal{G}_c = \frac{\sin^2(\pi/M)}{\lambda_0} \left[\frac{I_{m\,L_0}}{\prod_{i=1}^{N_0}\left(\epsilon_{i,0}/m\right)^{m\,q_{i,0}}} \times \prod_{p=1}^{R} \frac{I_{\kappa\,L_p}}{\prod_{i=1}^{\mathcal{N}_p}\left(\varepsilon_{i,p}/\kappa\right)^{\kappa\,\upsilon_{i,p}}}\right]^{1/(m\,L_0+\kappa\sum_{p=1}^{R}L_p)} \quad (42a)$$

and

$$\mathcal{G}_d = m\,L_0 + \kappa \sum_{p=1}^{R} L_p\,, \quad (42b)$$

respectively. Moreover, with respect to (41b), $\mathcal{G}_c$ and $\mathcal{G}_d$ are given by

$$\mathcal{G}_c = \sin^2\left(\frac{\pi}{M}\right) \times \left[I_{m\,L_0\,(R+1)} \prod_{\ell=0}^{R} \frac{\lambda_\ell^{-m\,L_0}}{\prod_{i=1}^{N_\ell}\left(\epsilon_{i,\ell}/m\right)^{m\,q_{i,\ell}}}\right]^{1/(m\,L_0\,(R+1))} \quad (42c)$$

and

$$\mathcal{G}_d = m\,L_0\,(R+1)\,, \quad (42d)$$

respectively. It should be noted that for a fixed $\gamma_{\rm p}$, i.e., $G \simeq \gamma_{\rm p}\,\sin^{-2}(\pi/M)$, the diversity-order approaches to zero due to the error floor. By comparing the above results for cases (*i*) and (*ii*), we may conclude that the e2e performance for high SNR depends mainly on the characteristics of the "less and worse" channels hop. For cases (*i*) and (*ii*), the worse channels are all these ones considered in the first and second hop, respectively.

### B. Optimal Power Allocation

Two power optimization strategies are next presented that can be used either separately or in a combination.

*1) Per Node Optimization:* In order to lower the energy consumption per transmitting node, let us now limit the total transmission energy per symbol and per channel block for the $\ell$th transmitting node as

$$K\,\lambda_\ell\,E_{\rm p} + (W_\ell - K)\;\lambda_\ell\,E_{\rm s} \le E_T(\ell)\,, \quad (43)$$

with $E_T(\ell)$ being the predetermined energy threshold of the $\mathcal{S} \to \mathcal{D}$ ($\ell = 0$) or $\mathcal{R}_\ell \to \mathcal{D}$ ($\ell \neq 0$) links and $W_\ell > K$ being the $\ell$th channel block length. Also, let define the percentage of the pilot symbols energy per block of the $\ell$th link as

$$\beta_\ell = \frac{K\,\lambda_\ell\,E_{\rm p}}{E_T(\ell)}\,, \quad (44)$$

with $0 < \beta_\ell < 1 \; \forall \ell$. Then, in order to minimize (32), the argument

$$J_\ell = \left(\frac{\gamma\,\gamma_{\rm p}}{\gamma+\gamma_{\rm p}}\right)^{-1} = \frac{E_{\rm s}+K\,E_{\rm p}}{K\,E_{\rm s}\,E_{\rm s}} \quad (45)$$

should be minimized. Using (43) and (44), (45) can be expressed as

$$J_\ell = \frac{1+\beta_\ell\,(W_\ell-K-1)}{\beta_\ell\;(\beta_\ell-1)\;E_T(\ell)/\lambda_\ell}\,. \quad (46)$$

After setting the first derivative of $J_\ell$ with respect to $\beta_\ell$ equal to zero, the optimum $\beta_\ell$ is given by

$$\widehat{\beta}_\ell = \frac{\sqrt{W_\ell-K}-1}{W_\ell-K-1}\,. \quad (47)$$

Note that the optimal value of $\beta_\ell$ depends only on the information symbols length per block $W_\ell - K$. Note that a different power allocation strategy per link may be applied by following [8, Section V].

*2) Joint Optimization:* In order to minimize the e2e ASEP based on (8), OPA can be succeeded with respect to $\lambda_\ell$'s. Let $\boldsymbol{\lambda} = [\lambda_0\,\lambda_1\cdots\lambda_R]^T$ be the power allocation vector. Then, the minimization problem is formulated as follows:

$$\boldsymbol{\lambda}_{\rm opt} = \arg\min_{\boldsymbol{\lambda}} \{P_{se,e2e}\}\,, \quad (48a)$$

subject to

$$\sum_{\ell=0}^{R} \lambda_\ell = 1 \quad (48b)$$

and

$$0 < \lambda_\ell < 1,\; \forall \ell = 0, 1, \ldots, R. \quad (48c)$$

$$\hat{\lambda}_0 = \frac{\frac{B}{\Omega_{rd}} + \frac{3\,A\,B}{G\,\Omega_{sr}\,\Omega_{rd}} - \frac{4\,A^2}{\Omega_{sr}} + \sqrt{\left(\frac{B}{\Omega_{rd}} + \frac{3\,A\,B}{G\,\Omega_{sr}\,\Omega_{rd}} - \frac{4\,A^2}{\Omega_{sr}}\right)^2 - \frac{16\,A}{\Omega_{sr}}\left(\frac{B}{\Omega_{rd}} - \frac{A^2}{\Omega_{sr}}\right)\left(\frac{B}{G\,\Omega_{rd}} - A\right)}}{4\left(\frac{B}{\Omega_{rd}} - \frac{A^2}{\Omega_{sr}}\right)} \tag{51}$$

In general, the above nonlinear optimization problem can be solved using numerical techniques. Hence, a generic analytical solution can not be derived.

As a case study here, we limit our analysis to one relay. Using (38) for independent and identically distributed Nakagami fading with $L_\ell = L$ and $m_\ell = \kappa_p = m$, $\forall \ell, p$, the e2e ASEP is given by

$$P_{se,e2e} = \frac{G^{-2\,m\,L}}{\left(\frac{\Omega_{sd}}{m}\right)^{m\,L}} \times \left( \frac{I_L^2}{\left(\frac{\Omega_{sr}}{m}\right)^{m\,L} \lambda_0^{2\,m\,L}} + \frac{I_{2\,L}}{\left(\frac{\Omega_{rd}}{m}\right)^{m\,L} \lambda_0^{m\,L}\,\lambda_1^{m\,L}} - \frac{G^{-m\,L}\,I_{2\,L}\,I_L}{\left(\frac{\Omega_{sr}}{m}\,\frac{\Omega_{rd}}{m}\right)^{m\,L} \lambda_0^{2\,m\,L}\,\lambda_1^{m\,L}} \right), \tag{49}$$

where $\Omega_{0,i} = \Omega_{sd}$, $\Theta_{1,i} = \Omega_{sr}$ and $\Omega_{1,i} = \Omega_{rd}$ stand for the $\mathcal{S} \to \mathcal{D}$, $\mathcal{S} \to \mathcal{R}_1$, and $\mathcal{R}_1 \to \mathcal{D}$ channel powers, respectively. Based on (49), the optimization problem in (48) with respect to $\lambda_0$ can be easily solved using standard minimization techniques ($\lambda_1 = 1 - \lambda_0$). Starting from $\mathrm{d}P_{se,e2e}(\lambda_0)/\mathrm{d}\lambda_0 = 0|_{\lambda_0 = \hat{\lambda}_0}$, and after some algebraic manipulations, we get

$$\hat{\lambda}_0^{m\,L}\,(2\,\hat{\lambda}_0 - 1)\,\frac{I_{2\,L}}{(\Omega_{rd}/m)^{m\,L}} + (3\,\hat{\lambda}_0 - 2)\,\frac{G^{-m\,L}\,I_{2\,L}\,I_L}{(\Omega_{sr}\,\Omega_{rd}/m^2)^{m\,L}} = \frac{2\,I_L^2}{(\Omega_{sr}/m)^{m\,L}}\,(1 - \hat{\lambda}_0)^{m\,L+1}. \tag{50}$$

Well-known root-finding techniques for polynomials must be applied in order to get a real root for $\hat{\lambda}_0$ in $(0, 1)$. For single-antenna reception ($L = 1$) and Rayleigh fading ($m = 1$), $\hat{\lambda}_0$ is given by (51) (at top of this page), where $A = I_1 = \frac{1}{\pi}\left(\frac{\pi}{4} - \xi\;{}_2F_1\left(\frac{1}{2}, -\frac{1}{2}; \frac{3}{2}; \xi^2\right)\right)$ and $B = I_2 = \frac{1}{\pi}\left(\frac{3\,\pi}{16} - \xi\;{}_2F_1\left(\frac{1}{2}, -\frac{3}{2}; \frac{3}{2}; \xi^2\right)\right)$. Note that, $\Omega_{sd}$ does not have any impact on the optimization of the power allocation. This finding has been also reported in [24].

## V. Numerical and Computer Simulation Results

In our numerical results and in order to simplify their presentation, we shall consider identical channel models for all hops, the same number of receive antennas, $L_\ell = L$ $\forall \ell = 0, 1, \ldots, R$, and $\Omega_{sd} = \Omega_{sr} = \Omega_{0,j} = \Theta_{p,j} = 1$ and $\Omega_{rd} = \Omega_{p,j} = 10$ $\forall p = 1, 2, \ldots, R$ and $j = 1, 2, \ldots, L$. Moreover, for correlated fading channels, the exponential correlation model is adopted with $\varrho_{p,i,j} = \rho_{\ell,i,j} = \rho^{|i-j|}$ $\forall i, j = 1, 2, \ldots, L$, while identical Nakagami fading parameters, $m_\ell = \kappa_p = m$ $\forall \ell, p$, are assumed.

Fig. 1 presents curves for the exact e2e ABEP of a BPSK pilot-symbols assisted system versus the total average SNR per branch and per bit, $\gamma$, using (8) with (24) and (28) (solid curves). A dual-hop system is considered with a single relay ($R = 1$), $\lambda_0 = 0.7$ and $\lambda_1 = 0.3$, dual-branch MRC ($L = 2$), correlated Nakagami fading and different values

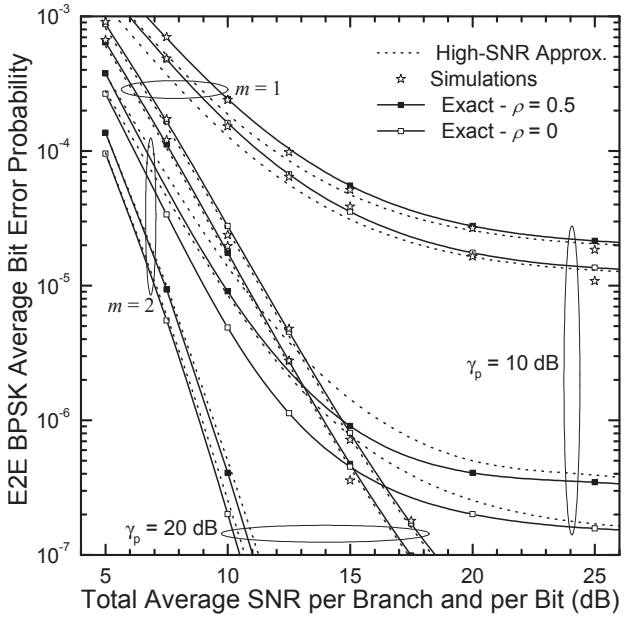


Fig. 1. E2e ABEP of BPSK versus average SNR per branch and per bit, $\gamma$, for a dual-hop system with dual-branch MRC/LSE, one relay, Nakagami fading, $\Omega_{sd} = \Omega_{sr} = 1$, $\Omega_{rd} = 10$, and different values of average PNR, $\gamma_{\mathrm{p}}$, Nakagami parameter, $m$, and exponential correlation coefficient, $\rho$.

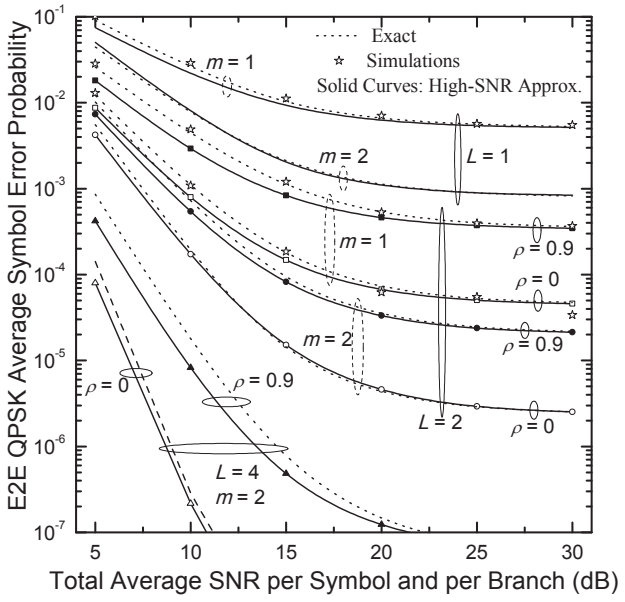


Fig. 2. E2e ASEP of QPSK versus total average SNR per branch and per symbol, $\gamma$, for a dual-hop system with MRC/LSE, $\gamma_{\mathrm{p}} = 10$ dB, $\Omega_{sd} = \Omega_{sr} = 1$, $\Omega_{rd} = 10$, two relays, exponential correlation and different values of number of branches $L$, correlation coefficient, $\rho$, and Nakagami parameter, $m$.

for the average PNR per pilot symbol and per time slot, $\gamma_{\mathrm{p}}$, Nakagami fading parameter, $m$, and correlation coefficient, $\rho$. It is obvious that the ABEP performance significantly improves as $\gamma$, $\gamma_{\mathrm{p}}$ and/or $m$ increase. Clearly, an increase of $\gamma_{\mathrm{p}}$ significantly reduces the error floor. High-SNR approximate results (dotted curves) are also included in the same figure using (8) with (34) in order to verify their accuracy. From the

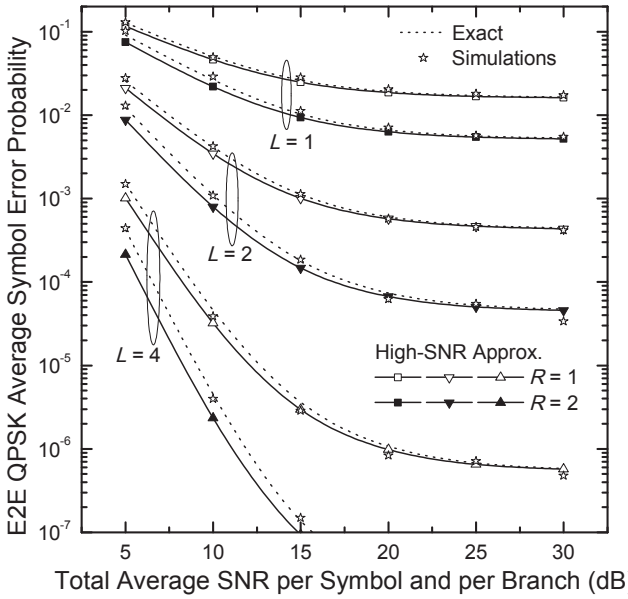


Fig. 3. E2e ASEP of QPSK versus total average SNR per branch and per symbol, $\gamma$, for a dual-hop system with MRC/LSE, $\gamma_{\rm p} = 10$ dB, $\Omega_{sd} = \Omega_{sr} = 1$, $\Omega_{rd} = 10$, independent Rayleigh fading and different values of number of branches $L$ and number of relays $R$.

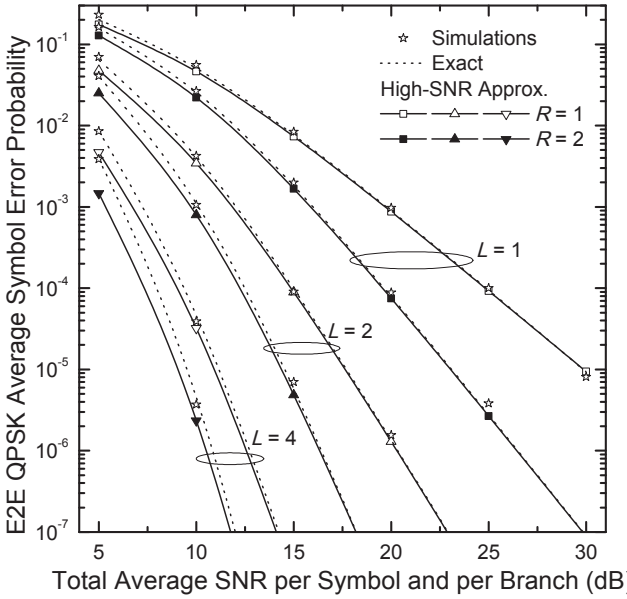


Fig. 4. E2e ASEP of QPSK versus total average SNR per branch and per symbol, $\gamma$, for a dual-hop system with MRC/LSE, $\gamma = \gamma_{\rm p}$, $\Omega_{sd} = \Omega_{sr} = 1$, $\Omega_{rd} = 10$, independent Rayleigh fading and different values of number of branches $L$ and number of relays $R$.

comparison with the exact ones it can be easily verified that (34) is highly accurate.

Similar conclusions can be drawn from Fig. 2 where e2e QPSK ASEP curves are presented as a function of the total average SNR per branch and per symbol for $\gamma_{\rm p} = 10$ dB, $R = 2$, $\lambda_0 = 0.5$, $\lambda_1 = 0.3$, and $\lambda_2 = 0.2$, and different values of $L$, $\rho$, and $m$. Both exact and high-SNR approximate curves are included for comparison purposes using (8) with (30) (dotted curves) and (34) (solid curves), respectively. As shown, the higher the $m$ and $L$ are, the better performance is achieved. Moreover, the ASEP performance is significantly degraded for highly correlated ($\rho = 0.9$) channels. Once again note the accuracy of the high-SNR curves as compared to the exact ones.

In Figs. 3 and 4 a comparison between the performances of two dual-hop systems with $R = 1$ and 2 is presented assuming independent Rayleigh channels. The main difference between these two figures is that in Fig. 3, $\gamma_{\rm p} = 10$ dB is fixed, while in Fig. 4, $\gamma_{\rm p}$ is equal to $\gamma$. From both figures it can be easily observed that as $R$ and/or $L$ increase, the performance improves, as expected. Moreover, from Fig. 3, the ASEP difference between two error floor levels (correspond to the same $L$) increases with increasing $L$. Fig. 4 demonstrates that for a given value of the e2e ASEP, the SNR difference between two curves (for $R = 1$ and 2 that correspond to the same $L$) decreases by increasing $L$. For example, for a fixed $P_{se,e2e} = 10^{-5}$, the SNR difference is about 7, 3 and 1.5 dB for $L = 1$, 2 and 4, respectively. It should be noticed that since $\gamma_{\rm p}$ equally increases with $\gamma$, no error floors are observed. From the above comparisons we may conclude that it is more beneficial to increase the number of antennas, instead of the number of relays.

In order to verify the correctness of the proposed analysis, in Figs. 1–4, Monte Carlo computer simulation results (star signs) for the exact e2e BPSK and QPSK ASEP are included for Rayleigh fading. From all these figures, it can be easily concluded that there is a perfect match between numerical exact and equivalent computer simulations results. Some notes regarding the implementation of the channel estimator developed in the context of our simulations are provided in the Appendix B.

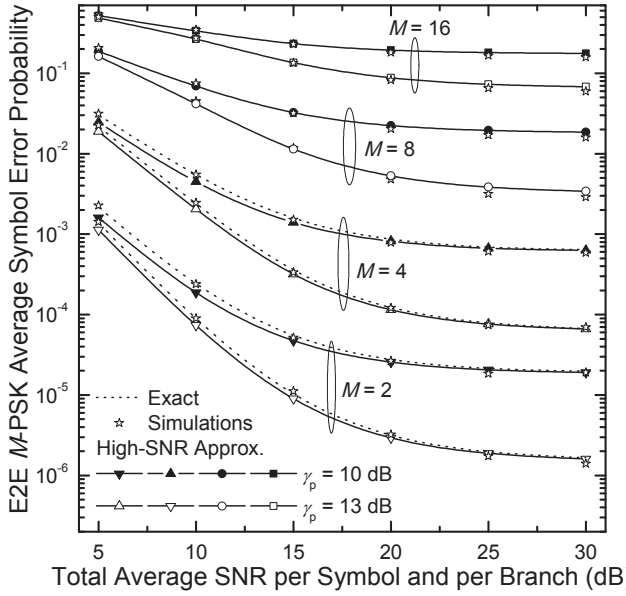


Fig. 5. E2e ASEP of $M$-PSK versus total average SNR per branch and per symbol, $\gamma$, for a dual-hop system with MRC/LSE, $\Omega_{sd} = \Omega_{sr} = 1$, $\Omega_{rd} = 10$, correlated Rayleigh fading, $\rho = 0.5$, and different values of the average PNR, $\gamma_{\rm p}$, and diversity order $M$.

Fig. 5 presents approximate e2e $M$-PSK ASEP curves (solid curves) as a function of $\gamma$ for $L = 2$, correlated Rayleigh channel with $\rho = 0.5$, and different values of $\gamma_{\rm p}$ and the modulation order, $M$. Exact results are plotted for BPSK and QPSK (dotted curves), while equivalent computer simulation results for the exact e2e ASEP, denoted with star signs, are included for all $M$'s. As expected, for fixed $\gamma$, the higher

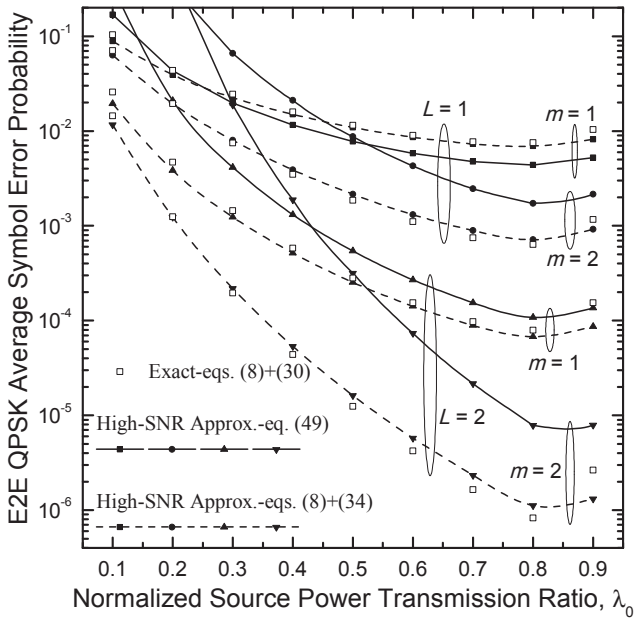


Fig. 6. E2e ASEP of QPSK versus normalized source power transmission ratio, $\lambda_0$, for a dual-hop system with MRC with LSE, $\gamma = \gamma_{\rm p} = 15$ dB, one relay, Rayleigh fading, $\gamma = 15$ dB, $\Omega_{sd} = \Omega_{sr} = 1$, $\Omega_{rd} = 10$, and different values of number of branches, $L$, and, fading parameter, $m$.

the $\gamma_{\rm p}$ and/or the lower the $M$ are, the better performance is obtained. Moreover, the highest difference between the error floor levels correspond to the same $M$ is succeeded for $M = 2$, while as $M$ increases this difference decreases. From this figure it can be concluded that our approximate results are highly accurate for any value of $M$.

In Fig. 6 approximate e2e ASEP curves of QPSK versus the normalized source transmission power ratio, $\lambda_0$, are presented (using (8) with (34) for dotted curves and (49) for solid curves) for a dual-hop system, $\gamma = \gamma_{\rm p} = 15$ dB, $R = 1$, independent Rayleigh fading, and different values of $L$ and $m$. From this figure we observe that (49), and consequently, (50) are highly accurate in finding the optimum $\lambda_0$ that minimizes the e2e ASEP. This conclusion is further supported from the comparison with exact results that are included in the same figure (square signs) and which are plotted using (8) with the help of (30). From this comparison we may conclude that there is a perfect match in the numerical evaluation of the e2e ASEP using either (30) or (34).

## VI. Conclusions

The e2e error rate performance of dual-hop communication networks, based on PSAM $M$-PSK, was analyzed directly from the distribution of the inner product of two complex Gaussian random vectors. In order to consider not-necessarily identical relay transmission powers, a key point in our analysis was the introduction of a new theorem for the joint CF of the real and imaginary parts of the inner product of two independent complex Gaussian random vectors. The selective-DF protocol was adopted, while we considered that the relays are equipped with an arbitrary number of receive antennas. It was also assumed that each relay estimates the CSI using the LSE technique by means of pilot symbols. Then, coherent detection based on the MRC scheme is performed. Our analysis was generic enough and could include any time- and space-correlated channel model per hop, not-necessarily identical channels, and arbitrary number of antennas per receiving end. The only requirement was that it should be readily available the CF of the sum of squared fading envelopes for the channel models under consideration. As a case study we specifically considered arbitrarily correlated Nakagami fading channels, where exact closed-form as well as analytical ASEP expressions were presented for BPSK and QPSK, respectively, while tight high-SNR approximate expressions were obtained for higher-order $M$-PSK modulation formats. These expressions helped us to extract the cooperation-gain and diversity-order. The OPA was also investigated and different power allocation strategies were proposed.

## Appendix A
## Proof of Theorem 1

Below is presented the proof of Theorem 1.

*Proof:* Let $x_i \sim \mathcal{CN}(\mu_{x_i}, \sigma^2_{x_i})$ and $y_i \sim \mathcal{CN}(\mu_{y_i}, \sigma^2_{y_i})$ be two independent complex Gaussian rvs from $\mathbf{x}$ and $\mathbf{y}$, respectively. We define a new set of $L$ random variables $w_i = q_i\, x_i$ distributed as $w_i \sim \mathcal{CN}(q_i\, \mu_{x_i}, |q_i|^2\, \sigma^2_{x_i})$. Then, the joint CF of $z_{\rho i} = \Re\{w_i\, y_i^*\}$ and $z_{\iota i} = \Im\{w_i\, y_i^*\}$ can be derived from [8, eq. (2)] as (A-1) (at the top of the next page). Let $w_j \sim \mathcal{CN}(q_j\, \mu_{x_j}, |q_j|^2\, \sigma^2_{x_j})$ and $y_j \sim \mathcal{CN}(\mu_{y_j}, \sigma^2_{y_j})$ be another group of independent rvs. Then, $w_j\, y_j^*$ is independent of $w_i\, y_i^*$, $\forall j \neq i$, since $w_i$, $y_i$, $w_j$, $y_j$ are mutually independent complex Gaussian rvs. Therefore, the joint CF of $z_{\rho j} = \Re\{w_j\, y_j^*\}$ and $z_{\iota j} = \Im\{w_j\, y_j^*\}$ is independent of the joint CF of $z_{\rho i}$ and $z_{\iota i}$ $\forall i \neq j$. Thus from (13), since $z$ can be written as

$$z = \sum_{i=1}^{L} q_i\, x_i\, y_i^* = \sum_{i=1}^{L} w_i\, y_i^*, \tag{A-2}$$

we can express $\Psi_{z_\rho, z_\iota}(\jmath\,\omega_1, \jmath\,\omega_2)$ as a product of $L$ joint CFs, i.e.,

$$\begin{aligned}\Psi_{z_\rho, z_\iota}(\jmath\,\omega_1, \jmath\,\omega_2) &= \mathcal{E}_{z_\rho, z_\iota}\left\langle \exp\left\{-\jmath\,(\omega_1\, z_\rho + \omega_2\, z_\iota)\right\}\right\rangle \\ &= \prod_{i=1}^{L} \Psi_{z_{\rho i}, z_{\iota i}}(\jmath\,\omega_1, \jmath\,\omega_2)\,,\end{aligned} \tag{A-3}$$

according to which yielding (14). ■

## Appendix B
## Implementation Details for the LSE

An ideal method has been used to estimate the complex channel gain from the pilot symbols. This method is based on the fast Fourier transform (FFT). Specifically, a low-pass interpolator of sinc-type impulse response and infinite-length buffer size has been implemented. In time domain, this method interpolates the samples between successive pilot symbols with frame duration $T_f = 1/(2f_D)$, with $f_D$ being the maximum Doppler frequency shift. More specifically, after extracting from the pilot symbols a samples vector with channel estimates, it is upsampled by a factor $W$, with $W = \lfloor T_f/T_s \rceil = \lfloor 1/(2\, f_D\, T_s) \rceil$ being the channel block length, $T_s$ being the symbol duration and $\lfloor\cdot\rceil$ standing for the closest rounded-down positive integer. Then, FFT is performed and all samples correspond to frequencies higher than $f_D$ are being set to zero. Finally, inverse FFT (IFFT) is performed

$$\Psi_{z_{\rho i},z_{\iota i}}\left(\jmath\,\omega_1,\jmath\,\omega_2\right)=\mathcal{E}_{z_{\rho i},z_{\iota i}}\left\langle\exp\left\{-\jmath\,\left(\omega_1\,z_{\rho i}+\omega_2\,z_{\iota i}\right)\right\}\right\rangle=\left(1+\frac{\omega_1^2+\omega_2^2}{4}\,|q_i|^2\,\sigma_{x_i}^2\,\sigma_{y_i}^2\right)^{-1}$$
$$\times\exp\left\{-\frac{\frac{\omega_1^2+\omega_2^2}{4}\,|q_i|^2\left(|\mu_{x_i}|^2\,\sigma_{y_i}^2+|\mu_{y_i}|^2\,\sigma_{x_i}^2\right)-\jmath\,\Re\left\{\left(\omega_1-\jmath\,\omega_2\right)\mu_{y_i}^*\,q_i\,\mu_{x_i}\right\}}{1+\frac{\omega_1^2+\omega_2^2}{4}\,|q_i|^2\,\sigma_{x_i}^2\,\sigma_{y_i}^2}\right\}\tag{A-1}$$

to get the interpolated complex gain channel estimates in the time domain.

## REFERENCES


[1] K. J. R. Liu, A. K. Sadek, W. Su, and A. Kwasinski, *Cooperative Communications and Networking*. Cambridge University Press, 2009.

[2] J. G. Proakis, "Probabilities of error for adaptive reception of $M$-phase signals," *IEEE Trans. Commun.*, vol. COM-16, no. 1, pp. 71–81, Feb. 1968.

[3] R. F. Pawula, S. O. Rice, and J. H. Roberts, "Distribution of the phase angle between two vectors perturbed by Gaussian noise," *IEEE Trans. Commun.*, vol. COM-30, no. 8, pp. 1828–1841, Aug. 1982.

[4] R. F. Pawula, "Distribution of the phase angle between two vectors perturbed by Gaussian noise II," *IEEE Trans. Veh. Technol.*, vol. 50, no. 2, pp. 576–583, Mar. 2001.

[5] W. M. Gifford, M. Z. Win, and M. Chiani, "Diversity with practical channel estimation," *IEEE Trans. Wireless Commun.*, vol. 4, no. 5, pp. 1935–1947, Jul. 2005.

[6] Y. Ma, R. Schober, and S. Pasupathy, "Effect of channel estimation errors on MRC diversity in Rician fading channels," *IEEE Trans. Veh. Technol.*, vol. 54, no. 6, pp. 2137–2142, Nov. 2005.

[7] J. M. Torrance and L. Hanzo, "Comparative study of pilot symbol assisted modem schemes," in *Proc. 1995 IEE Radio Receiv. Assoc. System Conf.*

[8] R. K. Mallik and N. C. Sagias, "Distribution of inner product of complex Gaussian random vectors and its applications," *IEEE Trans. Commun.*, vol. 59, no. 12, pp. 3353–3362, Dec. 2011.

[9] W. Yi and M. Pätzold, "Parameter optimization for amplify-and-forward relaying with imperfect channel estimation," in *Proc. 2009 IEEE Veh. Technol. Conf. – Spring.*

[10] S. Han, S. Ahn, E. Oh, and D. Hong, "Effect of channel-estimation error on BER performance in cooperative transmission," *IEEE Trans. Veh. Technol.*, vol. 58, no. 4, pp. 2083–2088, May 2009.

[11] B. Gedik and M. Uysal, "Impact of imperfect channel estimation on the performance of amplify-and-forward relaying," *IEEE Trans. Wireless Commun.*, vol. 8, no. 3, pp. 1468–1479, Mar. 2009.

[12] M. J. Taghiyar, S. Muhaidat, and J. Liang, "On the performance of pilot symbol assisted modulation for cooperative systems with imperfect channel estimation," in *Proc. 2010 IEEE Wirel. Commun. Networking Conf.*

[13] M. Seyfi, S. Muhaidat, and J. Liang, "Amplify-and-forward selection cooperation over Rayleigh fading channels with imperfect CSI," *IEEE Trans. Wireless Commun.*, vol. 11, no. 1, pp. 199–209, Jan. 2012.

[14] X. J. Zhang and Y. Gong, "On the diversity gain in dynamic decode-and-forward channels with imperfect CSIT," *IEEE Trans. Commun.*, vol. 59, no. 1, pp. 59–63, Jan. 2011.

[15] D. S. Michalopoulos, N. D. Chatzidiamantis, R. Schober, and G. K. Karagiannidis, "Relay selection with outdated channel estimates in Nakagami-$m$ fading," in *Proc. 2011 IEEE Internat. Conf. Commun.*

[16] O. Amin, S. S. Ikki, and M. Uysal, "On the performance analysis of multirelay cooperative diversity systems with channel estimation errors," *IEEE Trans. Veh. Technol.*, vol. 60, no. 5, pp. 2050–2059, Jun. 2011.

[17] S. S. Ikki and S. Aissa, "Impact of imperfect channel estimation and co-channel interference on regenerative cooperative networks," *IEEE Wireless Commun. Lett.*, vol. 1, no. 5, pp. 436–439, Oct. 2012.

[18] S. S. Ikki, S. Al-Dharrab, and M. Uysal, "Error probability of DF relaying with pilot-assisted channel estimation over time-varying fading channels," *IEEE Trans. Veh. Technol.*, vol. 61, no. 1, pp. 393–397, Jan. 2012.

[19] K. Dhaka, R. K. Mallik, and R. Schober, "Performance analysis of a multi-hop communication system with decode-and-forward relaying," in *Proc. 2011 IEEE Internat. Conf. Commun.*

[20] J. Proakis and M. Salehi, *Digital Communications*, 5th ed. McGraw-Hill, 2007.

[21] R. K. Mallik, "Distribution of inner product of two complex Gaussian vectors and its application to MPSK performance," in *Proc. 2008 IEEE Internat. Conf. Commun.*, pp. 4616–4620.

[22] ——, "A new statistical model of the complex Nakagami-$m$ fading gain," *IEEE Trans. Commun.*, vol. 58, no. 9, pp. 2611–2620, Sep. 2010.

[23] Q. T. Zhang, "Maximal-ratio combining over Nakagami fading channels with an arbitrary branch covariance matrix," *IEEE Trans. Veh. Technol.*, vol. 48, no. 4, pp. 1141–1150, Jul. 1999.

[24] A. K. Sadek, W. Su, and K. J. R. Liu, "Multinode cooperative communications in wireless networks," *IEEE Trans. Signal Process.*, vol. 55, no. 1, pp. 341–355, Jan. 2007.

[25] J. Gil-Pelaez, "Note on the inversion theorem," *Biometrika*, vol. 38, no. 3-4, pp. 481–482, Dec. 1951.

[26] N. G. Shephard, "From characteristic function to distribution function: a simple framework for the theory," *Econometric Theory*, vol. 7, no. 4, pp. 519–529, Dec. 1991.



**Nikos C. Sagias** (S'03-M'05-SM'11) was born in Athens, Greece in 1974. He received the BSc degree from the Department of Physics (DoP) of the University of Athens (UoA), Greece in 1998. The MSc and Ph.D. degrees in Telecommunication Engineering were received both from the UoA in 2000 and 2005, respectively. Since 2001, he has been involved in various National and European Research & Development projects for the Institute of Space Applications & Remote Sensing of the National Observatory of Athens, Greece. During 2006-2008, he was a research associate at the Institute of Informatics & Telecommunications of the National Centre for Scientific Research–"Demokritos," Athens, Greece. Currently, he is an Assistant Professor at the Department of Informatics and Telecommunications of the University of Peloponnese, Tripoli, Greece.

Dr. Sagias research interests are in the research area of wireless digital communications, and more specifically in MIMO and cooperative diversity systems, fading channels, and communication theory. In his record, he has over forty (40) papers in prestigious international journals and more than thirty (30) in the proceedings of world recognized conferences. He is an Editor for the IEEE TRANSACTIONS ON WIRELESS COMMUNICATIONS, while he acts as a TPC member for various IEEE conferences (GLOBECOM, VTC, WCNC, etc). He is a co-recipient of the best paper award in communications in the 3rd International Symposium on Communications, Control & Signal Processing (ISCCSP), Malta, March 2008. He is a senior member of the IEEE and member of the IEEE Communications Society as well as the Hellenic Physicists Association.